





## 14 **Abstract**

15           In California, it is essential to understand the evolution of water resources in response to a  
16 changing climate to sustain its economy and agriculture and build resilient communities. Although  
17 extreme conditions have characterized the historical hydroclimate of California, climate change  
18 will likely intensify hydroclimatic extremes by the End of Century (EoC). However, few studies  
19 have investigated the impacts of EoC extremes on watershed hydrology. We use cutting-edge  
20 global climate and integrated hydrologic models to simulate EoC extremes and their effects on the  
21 water-energy balance. We assess the impacts of projected driest, median, and wettest water years  
22 under a Representative Concentration Pathway (RCP) 8.5 on the hydrodynamics of the Cosumnes  
23 river basin. High temperatures ( $>2.5^{\circ}\text{C}$ ) and precipitation ( $>38\%$ ) will characterize the EoC  
24 extreme water years compared to their historical counterparts. Also, precipitation, mostly in the  
25 form of rain, is projected to fall earlier. This change reduces snowpack by more than 90%,  
26 increases peak surface water and groundwater storages up to 75% and 23%, respectively, and  
27 makes these peak storages occur earlier in the year. Because EoC temperatures and soil moisture  
28 are high, both potential and actual evapotranspiration (*ET*) increase. The latter, along with the lack  
29 of snowmelt in the warm EoC, cause surface water and groundwater storages to significantly  
30 decrease in summer, with groundwater showing the highest rates of decrease. Besides, the changes  
31 in the precipitation phase lead the lower-order streams to dry out in EoC summer whereas the  
32 mainstream experiences an increase in storage.

33 **Keywords:** future climate extremes, integrated hydrologic model, global climate model, end of  
34 century hydrology, watershed hydrology, water management



35           **Introduction**

36           California, the fifth largest economy in the world, hosts one of the largest agricultural  
37 regions in the United States and is home to over 39 million people. Because of its geographic  
38 location, Mediterranean climate, geology, and landscape, the state of California is sensitive to  
39 climate change (Hayhoe et al. 2004). Understanding how water resources will evolve under a  
40 changing climate is crucial for sustaining the state's economy and agricultural productivity. The  
41 region is especially susceptible to climate change given its reliance on the Sierra Nevada Mountain  
42 snowpack as a source of water supply (e.g., Dettinger & Anderson, 2015). Studies show that  
43 temperatures may warm by as much as 4.5°C by the End of Century (hereafter, EoC) (Cayan et  
44 al., 2008), and that snowpack is expected to decrease as most precipitation will fall as rain instead  
45 of snow and rain on snow events will exacerbate melt (Cayan et al., 2008; Gleick, 1987; Maurer,  
46 2007; Mote et al., 2005; Musselman, Clark, et al., 2017; Musselman, Molotch, et al., 2017;  
47 Rhoades, Ullrich, & Zarzycki, 2018a). Given that precipitation falls predominantly in winter  
48 months and the summers are hot and dry, the snow accumulated during the winter provides  
49 important water storage for the dry season and is crucial to meet urban demand, sustain ecosystem  
50 function, and maintain agricultural productivity (Bales et al., 2006; Dierauer et al., 2018). As such,  
51 any significant reduction in the snowpack will drastically affect the hydrology of the state (Barnett  
52 et al., 2005; Harpold & Molotch, 2015; Milly et al., 2005; Rhoades et al., 2018 a,b).

53           Over the past several decades, researchers have worked to understand how changes in  
54 Sierra Nevada snowpack during both dry and wet periods will affect evapotranspiration (Tague &  
55 Peng, 2013) and streamflow (Berghuijs et al., 2014; Gleick, 1987; He et al., 2019; Maurer, 2007;  
56 Safeeq et al., 2014; Son & Tague, 2019; Vicuna & Dracup, 2007; Vicuna et al., 2007). Analyses  
57 of recent historical trends show that reductions in snowpack result in increases in winter



58 streamflow and decreases in the summer streamflow (e.g. Safeeq et al., 2012). However, the  
59 sensitivity of a given area to these climatic changes depends on many factors including geology  
60 and therefore drainage efficiency, topography, and land cover (Alo & Wang, 2008; Christensen et  
61 al., 2008; Cristea et al., 2014; Ficklin et al., 2013; Mayer & Naman, 2011; Safeeq et al., 2015; Son  
62 & Tague, 2019; Tang et al., 2019).

63 Climate change in California is also expected to lead to unprecedented extreme conditions,  
64 which include both severe drought and intense deluge (Swain et al., 2018). In recent years, these  
65 changes have already been observed in the forms of multi-year droughts (Cook et al., 2004; Griffin  
66 & Anchukaitis, 2014; Shukla et al., 2015) and high-intensity precipitation events mainly caused  
67 by atmospheric rivers (Dettinger et al., 2004; Dettinger, 2011; Dettinger, 2013; Ralph & Dettinger,  
68 2011; Ralph et al., 2006). Periods without regular precipitation will require water management  
69 strategies to adapt to ensure demands are met. Similarly, risk management plans and/or  
70 infrastructure for floods, landslides, and other water surplus associated hazards (such as dam  
71 failure) may also require reconsideration. This will be especially true if periods of precipitation,  
72 including those associated with atmospheric rivers, become more extreme, variable, and occur  
73 over a shorter window of time (Swain et al., 2018; Gershunov et al., 2019; Huang et al., 2020;  
74 Rhoades et al., 2020b; Rhoades et al., 2021). Changes in water availability due to climate  
75 “whiplash” will also have important ramifications for water resource management (Wang et al.,  
76 2017; Swain et al., 2018) and significantly increase annual flood damages based on the level of  
77 global warming that occurs (Rhoades et al., 2021). For example, in just the last two decades,  
78 California has experienced the most severe drought in the last 1200 years (Griffin & Anchukaitis,  
79 2014) followed by the wettest year on record (Di Liberto, 2017; SCRIPPS, 2017). These changes  
80 in meteorological patterns may become the “new normal”, raising several outstanding questions



81 related to how these changes in climate will impact the integrated hydrologic cycle, and  
82 subsequently water resource availability for humans and ecosystems.

83 To project how changes in climate will impact watershed behavior, high-resolution,  
84 physics-based models are one of the most promising ways to simulate system dynamics accurately,  
85 particularly those that are non-linear, and constitute a better way to analyze a no-analog future than  
86 the models used in the previous works. Previous studies analyzed future hydrologic conditions in  
87 California but relied on models that do not 1) account for the interactions, feedbacks, and  
88 movements of water from the lower atmosphere to the subsurface; 2) represent groundwater  
89 dynamics and lateral flow; 3) incorporate physics-based high-resolution climate models and/or 4)  
90 account for decision-relevant model resolutions (e.g., Berghuijs et al., (2014); Gleick, (1987); He  
91 et al., (2019); Maurer, (2007); Safeeq et al., (2014); Son & Tague, (2019); Vicuna & Dracup,  
92 (2007); Vicuna et al., (2007)). Considerations of coupled interactions which explicitly account for  
93 groundwater connections are important (Condon et al., 2020, 2013; Maxwell and Condon, 2016),  
94 especially given groundwater is the largest reservoir in the terrestrial hydrologic budget and  
95 integral to water resource availability. Also, previous studies have focused on the mid-century  
96 period (e.g. Maurer & Duffy, 2005; Son & Tague, 2019), which may indicate a more muted signal  
97 in hydrologic impacts than at EoC. Understanding these impacts are essential because long-term  
98 climate projections show that extremes will be more frequent and significant by the EoC (Cayan  
99 et al., 2008).

100 In this work, we assess the impacts of EoC extremely dry and intensely wet conditions on  
101 the hydrodynamics of a Californian watershed that contains one of the last naturally flowing rivers  
102 in the state. This allows us to investigate the impacts of climate change without the complexity of  
103 active water management, and thus to set the context for water management decisions. We



104 specifically investigate how the water and energy balance respond to climate extremes under  
105 climate change, and how those changes propagate to alter the spatiotemporal distribution of water  
106 in different compartments of the watershed. We focus our investigation on the changes in  
107 groundwater and surface water storages. The balance of these two natural reservoirs, and their  
108 relationship in response to changes in snowpack reservoir changes, is important for water  
109 management decision making. We aim to 1) strengthen our physics-based understanding of the  
110 main hydrologic processes controlling changes in hydrologic storages under a changing climate,  
111 2) quantify the magnitude and timing of these shifts in storage, and 3) identify the areas that are  
112 most vulnerable to climate change.

113 To do so, we utilize a novel combination of cutting-edge climate and hydrologic model  
114 simulations. We use an integrated hydrologic model (ParFlow-CLM; Maxwell & Miller, 2005),  
115 which solves the water-energy balance across the Earth's critical zone. When projecting  
116 hydrologic flows, ParFlow-CLM's explicit inclusion of three-dimensional groundwater flow is  
117 important given its demonstrated role in impacting land surface processes like evapotranspiration  
118 (Maxwell & Condon, 2016). We drive Parflow-CLM with climate forcing from a physics-based,  
119 variable-resolution enabled global climate model (the Variable Resolution enabled Community  
120 Earth System Model, VR-CESM; Zarzycki et al., 2014) that dynamically couples multi-scale  
121 interactions within the atmosphere-ocean-land system. This novel pairing of models allows for  
122 several key considerations not present in other methods. Our approach represents both dynamical  
123 and thermodynamic atmospheric response to climate change across scales, different from "pseudo-  
124 global warming" and "statistical delta" approaches used in many hydrologic modeling studies  
125 (e.g., Foster et al., 2020; Rasmussen et al., 2011). While these approaches are useful to isolate the  
126 impact of a given perturbation and/or variable, expected changes in climate will involve the co-



127 evolution of many processes, and may therefore not account for compensating factors. The  
128 interaction between dynamical and thermodynamic responses has important, and sometimes,  
129 offsetting effects on features such as atmospheric rivers. For example, Payne et al. (2020) show  
130 that the thermodynamic response to climate change enhances atmospheric river characteristics  
131 (e.g., Clausius-Clapeyron relationship), whereas the dynamical response diminishes atmospheric  
132 river characteristics (e.g., changes in the jet stream and storm track landfall location). Therefore,  
133 VR-CESM may simulate a more inclusive hydroclimatic response to climate change in the western  
134 United States at a resolution that is at the cutting-edge of today's global climate modeling  
135 capabilities for decadal-to-centennial length simulations (Haarsma et al., 2016).

136 We perform these couplings on spatial and temporal scales relevant for atmosphere-to-  
137 land, and land-to-subsurface interactions, an important consideration, given the recent work  
138 showing the importance of meteorological forcing resolution in representing the hydrologic cycle  
139 (Kampenhout et al., 2019; Maina et al., 2020b; Rhoades et al., 2016; Rhoades, Ullrich, Zarzycki,  
140 et al., 2018c; Wu et al., 2017). Climate conditions for EoC (2070-2100) and a 30-year historical  
141 period (1985-2015) are simulated to identify the median, wettest, and driest water year (WY) in  
142 each. We then simulate the subsequent watershed hydrology of each year using ParFlow-CLM  
143 forced with the meteorological conditions of each of the WYs.

144

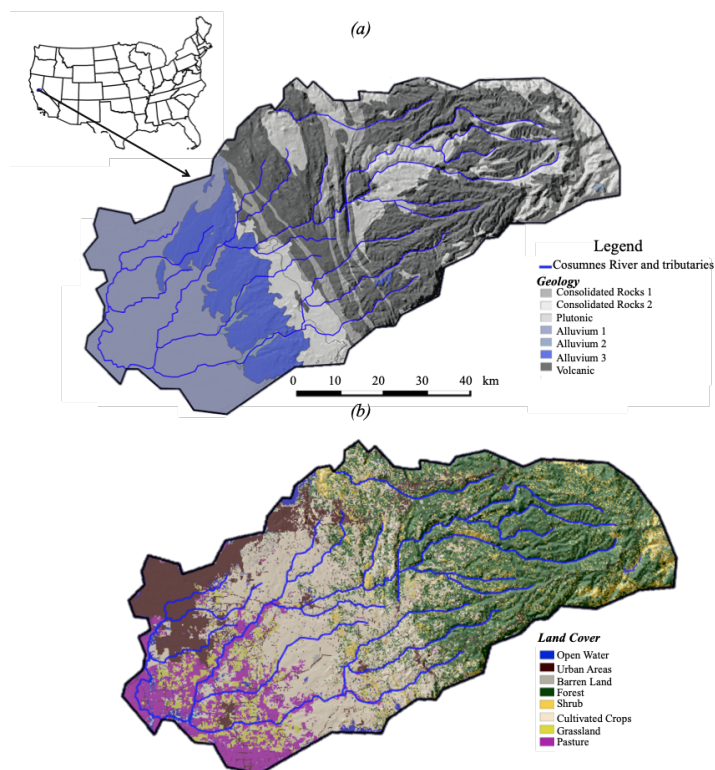
### 145 **1. The Cosumnes watershed**

146 The Cosumnes River is one of the last rivers in the western United States without a major  
147 dam, offering a rare opportunity to isolate the impacts of a changing climate on the hydrodynamics  
148 without reservoir management consideration (Maina et al., 2020a; Maina and Siirila-Woodburn,  
149 2020). The watershed spans the Central Valley-Sierra Nevada interface and therefore represents



150 important aspects of the large-scale hydrology patterns of the state, namely the assessment of  
151 interactions between changes in precipitation, snowpack, streamflow, and groundwater across  
152 elevation and geologic gradients. Located in Northern California, USA, the Cosumnes watershed  
153 is approximately 7,000 km<sup>2</sup> in size (Figure 1) and is between the American and the Mokelumne  
154 Rivers. Its geology ranges from low-permeability rocks typical of the Sierra Nevada landscape  
155 (volcanic and plutonic) to the porous and permeable alluvial depositions of the Central Valley  
156 aquifers. These are separated by very low-permeability marine sediments. The watershed  
157 topography includes a range of landscapes typical of the region (e.g. varying from flat agricultural  
158 land, rolling foothills, and steep mountainous hillsides), and elevation varies from approximately  
159 2500 m in the upper watershed to sea level in the Central Valley (Figure 1). The Sierra Nevada  
160 mountains are characterized by evergreen forest while the Central Valley hosts an intensive  
161 agricultural region including crops such as alfalfa, vineyards, as well as pastureland. Like other  
162 Californian watersheds, the climate in the Cosumnes is Mediterranean consisting of wet and cold  
163 winters (with a watershed average temperature equal to 0°C) and hot and dry summers (with  
164 watershed average temperature reaching 25°C) (Cosgrove et al., 2003).





165

166 Figure 1: The Cosumnes Watershed (a) location and geology (Jennings et al., 1977), the alluvium  
167 in blue corresponds to the Central Valley aquifers whereas the consolidated rocks in gray  
168 correspond to the Sierra Nevada and cross-cutting marine sediments, and (b) land cover (Homer  
169 et al., 2015).

170

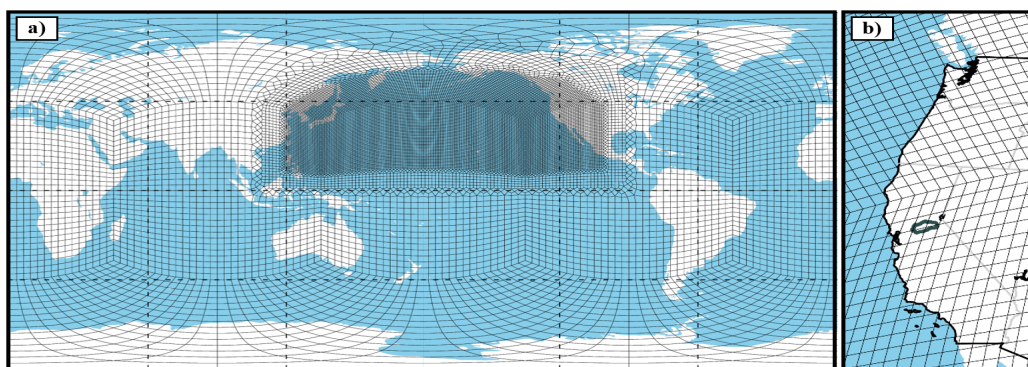
## 171 2. Experimental Design

### 172 2.1. Variable Resolution Community Earth System Model (VR-CESM)

173 Historical and EoC meteorological forcings are obtained from a simulation using the VR-  
174 CESM at a regionally refined resolution of 28 km over the Northern Pacific Ocean through the  
175 western United States, including the Cosumnes watershed and a global resolution of 111 km



176 (Figure 2). CESM has been jointly developed by NCAR (National Center for Atmospheric  
177 Research) and the DOE (U.S. Department of Energy) and simulates a continuum of Earth system  
178 processes including the atmosphere, land surface, land ice, ocean, ocean waves, and sea ice and  
179 the interactions between them (Collins et al., 2006; Gent et al., 2011; Hurrell et al., 2013). VR-  
180 CESM is a novel tool to perform dynamical downscaling as it allows for the interactions between  
181 the major components of the global climate system (e.g., atmosphere, cryosphere, land surface,  
182 and ocean) while allowing for regional-scale phenomena to emerge where regional refinement is  
183 applied, all within a single model (Huang et al., 2016; Rhoades et al., 2016; Rhoades, Ullrich, &  
184 Zarzycki, 2018b; Rhoades, Ullrich, Zarzycki, et al., 2018c).



185  
186 Figure 2: Variable Resolution Community Earth System Model (VR CESM) grid for (a) globe and  
187 (b) coastal western US with the Cosumnes watershed overlaid in dark gray.

188

189 The atmospheric model used for these simulations is the Community Atmosphere Model  
190 (CAM) version 5.4 with the spectral element dynamical core, with an atmospheric dynamics time  
191 step of 75 seconds, an atmospheric physics time step of 450 seconds, a prognostic treatment of  
192 rainfall and snowfall in the microphysics scheme (Gettelman and Morrison, 2015) and run under  
193 Atmosphere Model Intercomparison Project (AMIP) protocols (Gates, 1992). AMIP protocols  
194 include coupling the atmosphere-land-surface models and monthly-prescribed sea-surface



195 temperatures and sea-ice extents. Simulations with VR-CESM are performed for 30-year periods  
196 based on the climates from a historical period (1985-2015) and an EoC period (2070-2100). EoC  
197 simulations, analogous to Rhoades, Ullrich, & Zarzycki, 2018, are bounded by estimates of future  
198 changes in ocean conditions derived from a fully-coupled bias-corrected CESM simulation  
199 (assuming historical ocean simulation biases will be similar in the future simulation) and forced  
200 by greenhouse gases and aerosol concentrations assumed in the RCP8.5 emissions scenario.  
201 Historical VR-CESM outputs have been compared with reanalyses and future VR-CESM outputs  
202 have been analyzed for shifts in hydrometeorological extremes in further detail in Rhoades et al.,  
203 2020 a,b. To couple the outputs with ParFlow-CLM, we regrid the unstructured 28km VR-CESM  
204 data over the Cosumnes watershed using bilinear interpolation in the Earth System Modeling  
205 Framework (Jones, 1999) to a final resolution of approximately 11 km (i.e. 57 grids over the  
206 Cosumnes watershed). Notably, each of the spectral elements in the VR-CESM grid, shown in  
207 Figure 1, has a 4x4 set of Gauss–Lobatto–Legendre (GLL) quadrature nodes where equations of  
208 the atmospheric model are solved (Herrington et al., 2019). Therefore, the actual resolution at  
209 which the atmospheric dynamics and physics are solved in VR-CESM are at higher-resolution  
210 (~28km) than is shown in Figure 1, making these some of the highest resolution global Earth  
211 system model simulations over California to date (Haarsma et al., 2016).

212 To identify if VR-CESM is fit for purpose to simulate historical dry, median, and wet WYs,  
213 and inform potential biases in future projections (over California and, more specifically, the  
214 Cosumnes watershed), we first conduct a model comparison to a widely used observational  
215 product, the Parameter-elevation Relationships on Independent Slopes Model (PRISM; Daly et al.,  
216 2008) at 4 km resolution analogous to Rhoades et al., (2020a). However, in this study, we focus  
217 our assessment of VR-CESM fidelity over California and the Cosumnes watershed. PRISM



218 provides daily precipitation, mean dewpoint temperature and maximum and minimum surface  
219 temperature, and vapor pressure. PRISM precipitation and temperature data spanning 1981-2019  
220 are compared with the VR-CESM 1985-2015 simulations. We note that a mismatch in time period  
221 (1981-2019 versus 1985-2015) is deliberate. VR-CESM is simulated under AMIP-protocols  
222 (bounded by monthly observed sea-surface temperatures and sea-ice extents), and therefore we do  
223 not expect VR-CESM to exactly recreate past historical WYs. However, we do expect that our  
224 30-year simulation can reasonably recreate the range of WY types over California and the  
225 Cosumnes, which is why we utilize the broader range of PRISM WYs that are available. For this  
226 comparison, we regrid the unstructured VR-CESM data to 4km resolution (the native resolution  
227 of PRISM) using the Earth System Modeling Framework (ESMF) Offline Re-gridding Weight  
228 Generator in the NCAR Command Language (NCL, 2021).

229         The comparison (discussed in appendix A) indicates that VR-CESM reasonably reproduces  
230 the historical WY conditions (i.e., interannual range of PRISM precipitation largely overlaps with  
231 the range of model bias simulated by VR-CESM). VR-CESM generally simulates a wetter  
232 historical period over the Cosumnes (range of bias of 1330 mm) relative to PRISM (range of  
233 interannual variability of 1320 mm). Basin-average minimum (421 mm) and maximum (1740 mm)  
234 WY accumulated precipitation are slightly larger than those of PRISM. Of relevance to this study,  
235 PRISM has shown notable uncertainties in the Sierra Nevada. Lundquist et al., 2015 showed that  
236 an underrepresentation of the most extreme storm total precipitation in the Sierra Nevada can result  
237 in an upper-bound uncertainty of 20% in WY accumulated precipitation in PRISM. Therefore, the  
238 wettest WY simulated by VR-CESM is well within the 20% uncertainty range of PRISM's wettest  
239 WY ( $1580 \pm 316$  mm). Further, differences in basin-average WY accumulated precipitation  
240 between VR-CESM and PRISM are non-significant using a t-test and assuming a p-value  $< 0.05$ .



241 As discussed in further detail below, we posit that atmospheric river-related precipitation is likely  
242 the driver of the wet bias mismatch with PRISM. However, we also note that the uncertainty  
243 bounds of the PRISM product WY precipitation totals in the Sierra Nevada are estimated to be  
244 upwards of ~20% too dry (e.g., Lundquist et al., 2015), particularly for extreme precipitation  
245 events such as atmospheric rivers and in mountainous terrain.

246

## 247 **2.2. Integrated Hydrologic Model: ParFlow-CLM**

248 The integrated hydrologic model ParFlow-CLM (Kollet & Maxwell, 2006; Maxwell, 2013;  
249 Maxwell & Miller, 2005) solves the transfer and interactions of water and energy from the  
250 subsurface to the lower atmosphere including: groundwater dynamics, streamflow, infiltration,  
251 recharge, evapotranspiration, and snow dynamics. The model describes 3D groundwater flow in  
252 variably saturated media with the Richards equation (equation 1, Richards, 1931) and 2D overland  
253 flow with the kinematic wave equation (equation 2).

$$254 \quad S_S S_W(\psi_P) \frac{\partial \psi_P}{\partial t} + \phi \frac{\partial S_W(\psi_P)}{\partial t} = \nabla \cdot [K(x) k_r(\psi_P) \nabla(\psi_P - z)] + q_s \quad (1)$$

255 Where is  $S_S$  the specific storage ( $L^{-1}$ ),  $S_W(\psi_P)$  is the degree of saturation (-) associated  
256 with the subsurface pressure head  $\psi_P$  (L),  $t$  is the time (T),  $\phi$  is the porosity (-),  $k_r$  is the relative  
257 permeability (-),  $z$  is the depth,  $q_s$  is the source/sink term ( $T^{-1}$ ) and  $K(x)$  is the saturated hydraulic  
258 conductivity ( $L T^{-1}$ ).

259 The kinematic wave equation is used to describe surface flow in two dimensions is defined  
260 as:

$$261 \quad -k(x) k_r(\psi_0) \nabla(\psi_0 - z) = \frac{\partial \|\psi_0, 0\|}{\partial t} - \nabla \cdot \vec{v} \|\psi_0, 0\| - q_r(x) \quad (2)$$



262 Where  $\psi_0$  is the ponding depth,  $\max(\psi_0, 0)$  indicates the greater term between  $\psi_0$  and 0,  $\vec{v}$  is  
263 the depth averaged velocity vector of surface runoff ( $L T^{-1}$ ),  $q_r$  is a source/sink term representing  
264 rainfall and evaporative fluxes ( $L T^{-1}$ ).

265 Surface water velocity at the surface in  $x$  and  $y$  directions, ( $v_x$ ) and ( $v_y$ ) respectively, is  
266 computed using the following set of equations:

$$267 \quad v_x = \frac{\sqrt{S_{f,x}}}{m} \psi_0^{\frac{2}{3}} \text{ and } v_y = \frac{\sqrt{S_{f,y}}}{m} \psi_0^{\frac{2}{3}} \quad (3)$$

268 Where  $S_{f,x}$  and  $S_{f,y}$  friction slopes along  $x$  and  $y$  respectively and  $m$  is the manning coefficient.  
269 ParFlow employs a cell-centered finite difference scheme along with an implicit backward Euler  
270 scheme and the Newton Krylow linearization method to solve these nonlinear equations. The  
271 computational grid follows the terrain to mimic the slope of the domain (Maxwell, 2013).

272 ParFlow is coupled to the Community Land Model (CLM) to solve the surface energy and  
273 water balance, which enables interactions between the land surface and the lower atmosphere and  
274 the calculation of key land surface processes governing the system hydrodynamics such as  
275 evapotranspiration, infiltration, and snow dynamics. CLM models the thermal processes by closing  
276 the energy balance at the land surface given by:

$$277 \quad R_n(\theta) = LE(\theta) + H(\theta) + G(\theta) \quad (4)$$

278 Where  $\theta = \phi S_w$  is the soil moisture,  $R_n$  is the net radiation at the land surface (E/LT) a  
279 balance between the shortwave (also called solar) and longwave radiation,  $LE$  is the latent heat  
280 flux (E/LT) which captures the energy required to change the phase of water to or from vapor,  $H$   
281 is the sensible heat flux (E/LT) and  $G$  is the ground heat flux (E/LT).

282 More information about the coupling between ParFlow and CLM can be found in Maxwell  
283 & Miller, (2005). CLM uses the following outputs of the VR-CESM model at 3-hourly resolution  
284 to solve the energy balance at the land surface: precipitation, air temperature, specific humidity,



285 atmospheric pressure, north/south and east/west wind speed, and shortwave and longwave wave  
286 radiation.

287 We constructed a high-resolution model of the Cosumnes watershed with a horizontal  
288 discretization of 200 m and vertical discretization that varies from 10 cm at the land surface to 30  
289 m at the bottom of the domain. The model has 8 layers, the first 4 layers represent the soil layers  
290 and the other four the deeper subsurface. The total thickness of the domain is 80 m to ensure  
291 appropriate representation of water table dynamics. Observed water table depths (as measured at  
292 several wells located in the Central Valley portion of the domain) vary between approximately 50  
293 m and the land surface through a multi-year time period (Maina et al., 2020a). Therefore, to be  
294 conservative for imposing the lower boundary layer, anything below 80 m is expected to remain  
295 fully saturated. The resulting model comprises approximately 1.4 million active cells and was  
296 solved using 320 cores in a high-performance computing environment. The Cosumnes watershed  
297 is bounded by the American and Mokelumne rivers. We, therefore, impose weekly varying values  
298 of Dirichlet boundary conditions along these borders to reflect the observed changes of river stage.  
299 The eastern part of the watershed corresponding to the upper limit in the Sierra Nevada is modeled  
300 as a no-flow (i.e., Neumann) boundary condition. Hydrodynamic parameters required to solve the  
301 surface and subsurface flows (e.g., hydraulic conductivity, specific storage, porosity, and  
302 van Genuchten parameters) are derived from a regional geological map (Geologic Map of  
303 California, 2015; Jennings et al., 1977) and a literature review of previous studies (Faunt et al.,  
304 2010; Faunt and Geological Survey (U.S.), 2009; Gilbert and Maxwell, 2017; Welch and Allen,  
305 2014). We use the 2011 National Land Cover Database (NLCD) map (Homer et al., 2015) to  
306 define land use and land cover required by CLM. We further delineate specific croplands (notably  
307 alfalfa, vineyards, and pasture) in the Central Valley by using the agricultural maps provided by



308 the National Agricultural Statistics Service (NASS) of the US Department of  
309 Agriculture's (USDA) Cropland Data Layer (CDL) (Boryan et al., 2011). Vegetation parameters  
310 are defined by the International Geosphere-Biosphere Programme (IGBP) database (IGBP, 2018).  
311 A complete description of the model parameterization can be found in Maina et al. (2020a). The  
312 model has been extensively calibrated and validated using various datasets, including remotely  
313 sensed data and ground measurements, which are however very sparse in the area. Model  
314 validation which consists in comparing both surface and subsurface hydrodynamics (groundwater  
315 and river stages) and land surface processes was performed over a period that includes extremely  
316 dry and wet years. The reasonable agreement between observations and simulated variables has  
317 allowed us to conclude that the model can capture these extreme dynamics. Annual average  
318 differences between simulated and measured river stages and groundwater levels vary between 0.4  
319 and 0.8 m and 0.47 to 3.73 m respectively. Key land surface processes (evapotranspiration, soil  
320 moisture, and snow dynamics) were also in agreement with remotely sensed values. For example,  
321 annual average differences between the measured and simulated snow water equivalent, soil  
322 moisture, and evapotranspiration are equal to 3mm, 0.2, and 0.036 mm/s respectively. Simulated  
323 key parameters controlling the snow dynamics such as peak snow and timing of snow ablation  
324 were also in agreement with remotely sensed data for both dry and wet years. More details about  
325 model calibration and validation can be found in previous publications (Maina et al., 2020a, Maina  
326 et al., 2020b; Maina and Siirila-Woodburn, 2020c). The model has also been successfully used in  
327 recent investigations of post-wildfire and climate extremes hydrologic conditions and to assess the  
328 role of meteorological forcing scale on simulated watershed dynamics (Maina et al., 2020a, b;  
329 Maina and Siirila-Woodburn, 2020c). Initial conditions for pressure-head were obtained by a spin-  
330 up procedure using the forcing of the historical median WY. We recursively simulated the





331 historical median WY forcing until the differences of storage at the end of the WY were less than  
332 1%, indicating convergence. This pressure head field is then used as the initial condition for each  
333 of the five WYs of interest (i.e. the EoC wet, EoC dry, historic wet, historic dry, EoC median).  
334 Though we acknowledge land cover alterations are expected to occur by the EoC (either naturally  
335 or anthropogenically), in this work we assume that the vegetation remains constant for both  
336 historical and EoC simulations for simplicity. Although outside of the scope of this work, future  
337 studies will investigate the impacts of an evolved land use/land cover, vegetation physiology, and  
338 resilience strategies to manage water resources. Further, while the Central Valley of California  
339 hosts intensive agriculture that is reliant on groundwater pumping for irrigation, we didn't  
340 incorporate pumping and irrigation in our model configuration. We did this with the assumption  
341 that groundwater pumping rates may substantially change in the future due to new demands,  
342 policies, regulations, and changes in land cover and land use and aim to provide an estimate of the  
343 natural hydrologic system response to climate change.

344

### 345 **2.3. Analysis of EoC hydrodynamics**

346 To investigate how the EoC climate extremes affect water storages, we investigate five  
347 hydrologic variables: Snow Water Equivalent (*SWE*), Evapotranspiration (*ET*), Pressure-head ( $\psi$ )  
348 distributions, and surface and subsurface water storage. Total groundwater (GW) storage is given  
349 by:

$$350 \quad \text{Storage}_{GW} = \sum_{i=1}^{n_{GW}} \Delta x_i \times \Delta y_i \times \Delta z_i \times \psi_i \times \left( \frac{S_{s_i}}{\phi_i} \right) \quad (5)$$

351 where  $n_{GW}$  is the total number of subsurface saturated cells (-),  $\Delta x_i$  and  $\Delta y_i$  are cell discretizations  
352 along the x and y directions (L),  $\Delta z_i$  is the discretization along the vertical direction the cell (L),  
353  $S_{s_i}$  is the specific storage associated with cell  $i$ ,  $\psi_i$  the pressure-head, and  $\phi_i$  is the porosity.



354 Total surface water (SW) storage which account for any water located at the land surface  
355 (i.e., any cell of the model with a pressure-head greater than 0) and includes river water or overland  
356 flow is calculated via:

$$357 \quad \text{Storage}_{SW} = \sum_{i=1}^{n_{SW}} \Delta x_i \times \Delta y_i \times \psi_i \quad (6)$$

358 where  $n_{SW}$  is the total number of cells with surface water i.e. with surface  $\psi$  greater than 0 (-), and  
359  $i$  indicates the cell.

360 We compare each EoC WY simulation to its corresponding historical WY counterpart and  
361 both the historical and EoC medians. This allows us to assess how EoC extremes change relative  
362 to what is currently considered an extreme condition as well as to “normal” in the relevant time.  
363 Comparisons are shown as a percent change ( $PC$ ) calculated using:

$$364 \quad PC_{i,t} = \frac{X_{projection_{i,t}} - X_{baseline_{i,t}}}{X_{baseline_{i,t}}} \times 100 \quad (3)$$

365 where  $X$  is the model output ( $ET$ ,  $SWE$ , or  $\psi$ ) at a given point in space ( $i$ ) at a time ( $t$ ),  $baseline$  is  
366 the selected simulation (historical median, EoC median, or historical extreme), and  $projection$   
367 represents the simulation obtained with the EoC extreme WYs (dry or wet).

368

### 369 **3. Results**

370 In this section, we present a subset of the outputs from VR-CESM (precipitation and  
371 temperature) to identify the extreme (dry and wet) and median WYs of interest. Changes in fluxes  
372 and storages over the course of each WY, as well as the spatial variability of these changes in two  
373 important periods of the WY (peak flow and baseflow) are also shown.

374

#### 375 **3.1. Selection of the median, dry, and wet WYs**



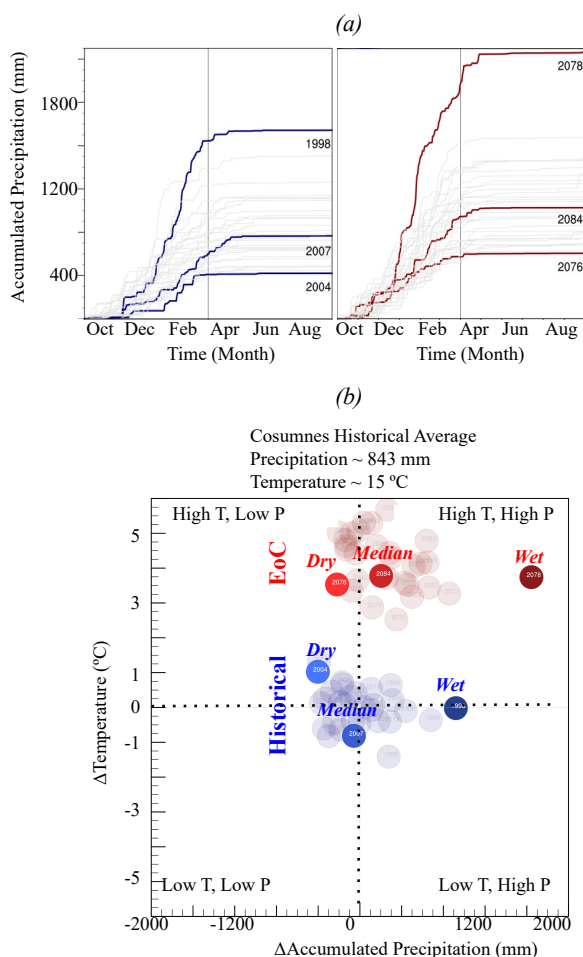
376 From the historical and EoC 30-year VR-CESM simulations we select the median, wettest,  
377 and driest WYs for comparison (see Figure 3a). Overall, the future WYs are ~30% wetter than the  
378 historical WYs (p-value ~0.006 for two-tailed t-test of equal average annual precipitation) in  
379 addition to being ~4.6°C warmer. Precipitation and temperature variances are mostly similar in the  
380 historical and EoC simulations, though EoC minimum temperature may be more variable (p-value  
381 ~0.059 for two-tailed f-test of equal variance in minimum temperature). On average the timing for  
382 the start, length, and end of precipitation is similar, though EoC precipitation may be less variable  
383 in its start time (p-value ~0.053 for f-test of equal variance in days to reach 5<sup>th</sup> percentile of annual  
384 precipitation). In the climate model, there are no clear trends between the precipitation timing  
385 metrics and total amount of precipitation.

386 The EoC median WY is much wetter than its historical counterpart, with about ~250 mm  
387 more precipitation that begins approximately 1 week earlier and ends approximately 2 weeks  
388 earlier in the year. The EoC wettest WY is much wetter than the historical wettest WY and is  
389 characterized by 42% more precipitation. This is consistent with Allan et al. (2020), who suggest  
390 a wetter future. The EoC wettest WY is 3.8°C warmer than the historical wettest WY and 4.6°C  
391 warmer than the historical median WY, as the historical median WY is one of the coolest years in  
392 the series. Precipitation occurs earlier in the EoC wet WY compared to the historical wet or median  
393 WYs, with the 5<sup>th</sup> percentile of precipitation reached 12 days earlier in the EoC wettest WY than  
394 either the wettest or median historical WYs. The duration of the EoC wettest WY precipitation  
395 season (146 days) is between the historical wettest WY (133 days) and the historical median WY  
396 (155 days).

397 The EoC dry WY is also much wetter than its historic counterpart; in fact, the EoC dry WY  
398 is wetter than the seven driest historical WYs of the 30-year historical ensemble. Simulation of 30



399 random draws from two identical normal distributions, repeated 100,000 times, finds that the  
400 lowest value in one is higher than the seven lowest values in the other only ~1.1% of the time (p-  
401 value ~0.011). This statistical test reveals that this VR-CESM simulation suggests that future dry  
402 years will be somewhat wetter than historical dry years. The EoC dry WY is only ~2.5°C warmer  
403 than the historical dry WY. The divergence in temperature is smaller for the comparison of EoC  
404 and historical WYs of the dry extremes as opposed to the wet extremes because the historical dry  
405 WY is the second-warmest WY in the historical simulations, while the EoC dry WY is the third  
406 coolest in the EoC simulations. Precipitation in the EoC dry WY starts particularly early, with the  
407 5<sup>th</sup> percentile of annual precipitation reached by mid-October. This is much earlier than either the  
408 dry or median historical WYs, which don't reach that percentile of precipitation until mid-to-late-  
409 November. The historical dry WY also has a particularly short precipitation duration of only 97  
410 days, while the EoC dry WY has a 163-day precipitation duration, more similar to the median  
411 historical WY duration of 155 days.



412  
413 Figure 3: (a) VR-CESM accumulated total precipitation for the historical and End of Century  
414 (EoC) simulations, and (b) quadrants for differences between each individual water year (WY)  
415 and the historical average temperature and accumulated precipitation in the Cosumnes watershed.  
416 The historical and EoC dry, median and wet WYs are indicated in blue and red, respectively.

417

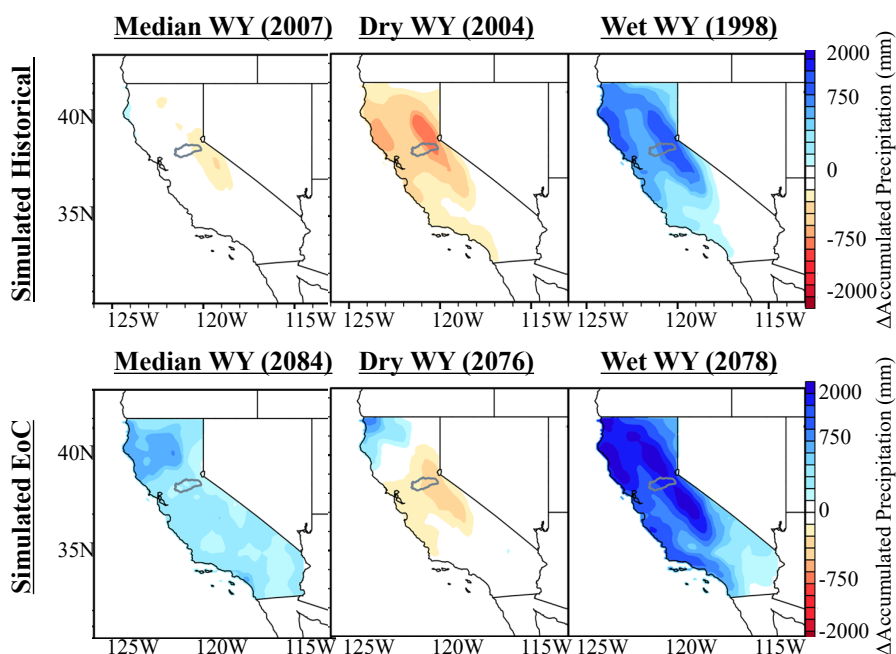
418 Figure 4 shows the spatial distribution of accumulated precipitation anomalies across  
419 California. These anomalies are computed for each of the six identified WYs relative to the  
420 climatological average (the 30-year historical mean). These spatial plots provide context for the



421 changes modeled in the Cosumnes watershed relative to broader precipitation changes California-  
422 wide. As in the Cosumnes, California-wide EoC dry, median, and wet WYs are all characterized  
423 by higher precipitation totals than their historical counterparts. Importantly, the EoC wet WY is a  
424 true outlier not only in the Cosumnes but across California too. California lies at an important  
425 large-scale circulation transition, namely semi-permanent high-pressure systems associated with  
426 the Hadley circulation. Therefore, how climate change alters the atmospheric dynamics over  
427 California, or more specifically how far northward storm-tracks may shift, remains uncertain and  
428 depends on climate model choice. This has led to papers that claim the future of California will be  
429 wet across a range of climate models (e.g., Neelin et al, 2013; Swain et al., 2013; Gershunov et al.,  
430 2019; Rhoades et al., 2020b; Persad et al., 2020) and, for select climate models, that it could be  
431 drier. Notably, these studies highlight an asymmetric response in the frequency of wet versus dry  
432 WYs (i.e., anomalously wet WYs increase in frequency much more in the future than anomalously  
433 dry WYs). Many of the aforementioned studies also highlight that in anomalously wet WYs  
434 extreme precipitation events (e.g., atmospheric rivers) will occur with greater intensity and  
435 frequency and largely drive changes in WY precipitation totals (which is shown in our VR-CESM  
436 simulations for California in more detail in Rhoades et al., 2020b). Given these complexities and  
437 others such as consideration for how dynamical and thermodynamical effects of climate change  
438 may interact with one another to offset or amplify extreme precipitation events (Payne et al., 2020),  
439 the hypothesis that global warming will result in a climate where the “wet gets wetter and dry gets  
440 drier” may be too simplistic of an assumption for California. Rhoades et al., (2020b) shows  
441 quantitatively that the increases in precipitation observed in the VR-CESM outputs are due to a  
442 greater number of intense atmospheric river events that occur more regularly back-to-back, which  
443 was recently corroborated by Rhoades et al. (2021) using uniform-high-resolution CESM



444 simulations at different warming scenarios, and that atmospheric river precipitation totals increase  
445 at a much larger rate (+53%/K) than non-AR precipitation totals (+1.4%/K), which agrees with  
446 findings made in other studies such as Gershunov et al. (2019).



447  
448 Figure 4: Precipitation spatial distributions of the dry, median, and wet water years (WY) for the  
449 30-year historical and EoC simulations relative to the climatological average (derived from the 30-  
450 year historical mean)

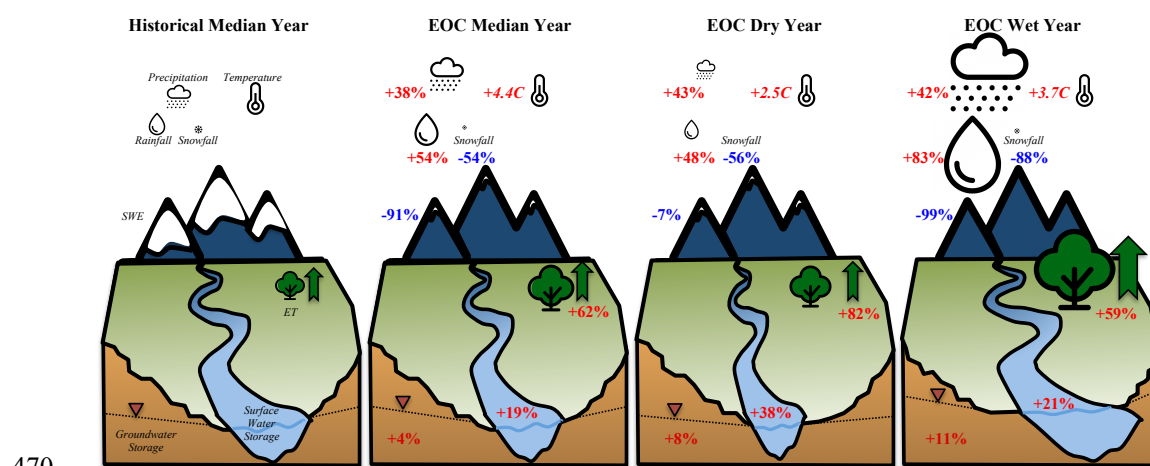
451

### 452 3.2. Changes in annual watershed-integrated fluxes and storages

453 Figure 5 illustrates the annual changes in the integrated hydrologic budget of the Cosumnes  
454 watershed for the EoC WYs (i.e., median, dry, and wet) compared to the historical median WY.  
455 The EoC median WY compared to the historical median WY has 38% more precipitation and the  
456 temperature is 4.4°C higher. Further, the precipitation phase also shifts with an increase in rainfall  
457 (54%) and a decrease in snowfall (-54%). This results in a significant decrease in *SWE* (-91%)



458 which is consistent with many other studies that have shown that increased temperatures due to  
 459 climate change will lead to low-to-no snow conditions (Berghuijs et al., 2014; Cayan et al., 2008;  
 460 Mote et al., 2005; Rhoades et al., 2018 a,b; Son & Tague, 2019). The increase in temperature and  
 461 precipitation results in an increase in *ET* (62%), consistent with the findings of other recent studies  
 462 (e.g. McEvoy et al., 2020). Nevertheless, the larger amount of precipitation associated with the  
 463 EoC is enough to offset higher *ET* demand and recharge groundwater and surface water, which  
 464 experience an increase of 4% and 19% respectively. The EoC wet WY has similar changes as the  
 465 EoC median WY when compared to the historical wet WY yet the magnitude of the increase in  
 466 surface (21%), and groundwater (11%) storages are higher due to more precipitation and higher  
 467 temperatures. The dry EoC WY is also characterized by higher precipitation (43%, the largest  
 468 increase) than its historical counterpart, this results in large increases in total groundwater (8%)  
 469 and surface water (38%) storages.



470  
 471 Figure 5: Annual percent changes in precipitation, rainfall, snowfall, temperature, *SWE*, *ET*,  
 472 surface water, and groundwater storages in the EoC water years (WY) (i.e median, dry, and wet)  
 473 at the watershed scale relative to their historical counterparts. Info-graphic size scaled to EoC  
 474 conditions.

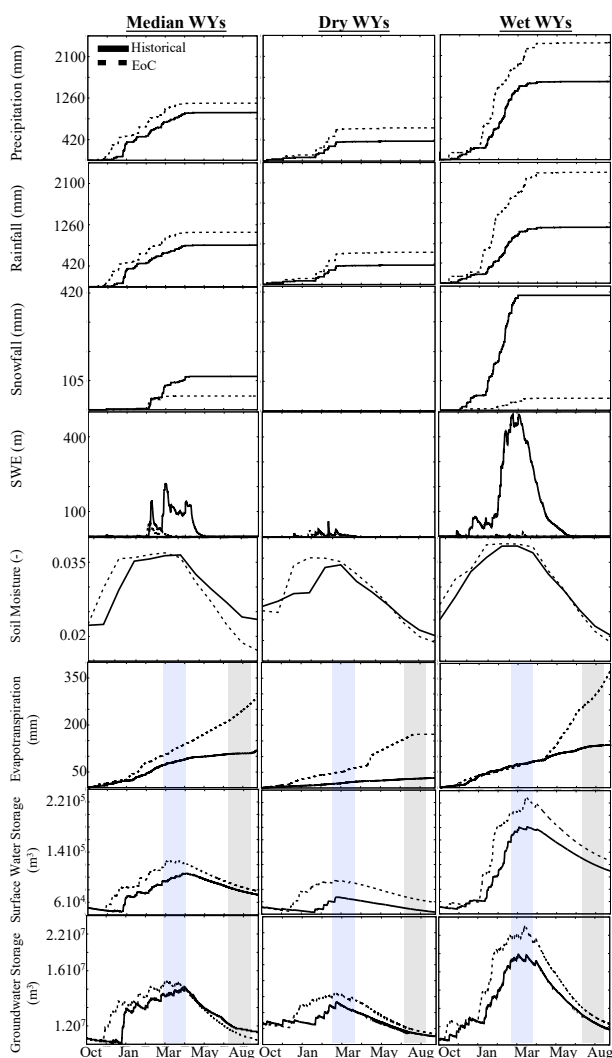




475

476 **3.3. Temporal variation of watershed-integrated fluxes and storages**

477 Understanding the annual changes at the watershed scale is important to broadly  
478 understand changes in the water budget in response to future climate extremes. However, a deeper  
479 understanding of the processes that drive these changes and the interactions from atmosphere-  
480 through-bedrock requires an analysis of their spatiotemporal variations as well. Figure 6 shows  
481 the temporal variations of each of the historical and EoC WY's integrated hydrologic budgets  
482 grouped by WY type (columns), with a top-down sequencing of hydrologic variables of interest in  
483 order from the atmosphere through subsurface (rows). This organization allows for the  
484 investigation of propagating impacts to be directly compared in time. In this section, we discuss  
485 historical vs EoC changes observed in each of the WY types (i.e., median, dry, and wet). Each WY  
486 shows unique hydrodynamic behaviors and changes compared to the historical conditions. The  
487 median WY sheds light on how changes in the precipitation phase and increases in temperature  
488 and precipitation in the EoC will impact the hydrodynamics. The dry WYs allow comparing EoC  
489 and historical low-to-no snow conditions whereas assessing the hydrodynamics of the EoC wet  
490 WY provides a better understanding of how intense EoC precipitation along with the warm EoC  
491 climate will shape the hydrology.



492

493 Figure 6: Temporal variations of the total cumulative precipitation, rainfall, and snowfall at the  
 494 watershed scale, total *SWE* at the watershed scale, the average watershed values of soil moisture,  
 495 the cumulative watershed *ET*, and the total surface water, and groundwater storages at the  
 496 watershed scale associated with the six historical and EoC Water Years (WY). The blue area  
 497 indicates the selected peak flow period while the gray area corresponds to the selected baseflow  
 498 conditions for the spatial distribution analyses.



499

### 500 **3.3.1. Median water years**

501 As indicated in section 3.1, the EoC median WY has more precipitation than the historical  
502 median WY. The EoC precipitation comes mainly as rain due to the warmer temperatures of the  
503 EoC and includes virtually no snowfall from late-winter to early-spring. This precipitation phase-  
504 change combined with the earlier snowfall cessation date in the WY results in minimal and even  
505 non-existent *SWE* in the Cosumnes watershed for much of the WY, a significant change compared  
506 to historic conditions. EoC peak *SWE* occurs in February in contrast to the historical peak *SWE*,  
507 which occurs in April. Due to the watershed's relatively low elevation, snow accumulates only in  
508 the upper part of the Cosumnes watershed (~10% of the total watershed area). Only areas located  
509 in the highest elevations (> 2000 m), such as the eastern limit of the watershed, show any *SWE* in  
510 the EoC simulations whereas in the historical WYs we observed *SWE* as low as 1000 m.

511 The decrease in snow and the increase in rain along with an earlier onset of seasonal  
512 precipitation directly impacts soil moisture, which sees an early increase with a slightly higher  
513 peak than historical. As more water is available earlier in the EoC, the *ET* demand from increased  
514 temperatures is met until substantially higher summer temperatures increase *ET* at a much faster  
515 rate than the historical WY. The high EoC *ET* and the lack of snowmelt cause the soil to rapidly  
516 dry from late-spring through late-summer.

517 Because of the marked increase in total precipitation and shift from snow to rain in the EoC  
518 simulations, surface water storage generally increases throughout the WY. This is consistent with  
519 previous studies (Gleick, 1987; He et al., 2019; Maurer, 2007; Safeeq et al., 2014; Son & Tague,  
520 2019; Vicuna & Dracup, 2007; Vicuna et al., 2007). Surface water storage increases in early  
521 November in the EoC simulations while in the historical simulations this increase occurs in



522 January. Similar to the earlier peak *SWE* and soil moisture, the peak surface water storage in the  
523 EoC is also earlier (January through February) compared to the historical period (March through  
524 April). This late-season surface water storage remains larger because the accumulated precipitation  
525 is large enough to overcome the increased *ET* in a warmer climate. Similar to surface water storage,  
526 groundwater storage increases earlier and peaks at a larger amount than the historical WY.  
527 However, in contrast to the surface water storage, the groundwater storage during baseflow  
528 conditions is lower in the median EoC compared to the median historical year. This decrease in  
529 groundwater during baseflow conditions is due to the lack of snowmelt and higher EoC *ET*. In  
530 late-spring and summer in the EoC, groundwater keeps depleting through *ET* and is not recharged  
531 by snowmelt through surface and subsurface flows from the Sierra Nevada as in the historical  
532 period. This may indicate that compared to surface water storages, groundwater storage may be  
533 more sensitive to EoC hydroclimatic changes (which are multi-fold, and in this case include an  
534 increase in precipitation, a transition from snow to rain, and higher *ET*). One way to quantitatively  
535 measure this sensitivity is to compare the seasonal change in water storage between peak and  
536 baseflow conditions. Historically, changes between peak and baseflow conditions (i.e., the amount  
537 of water lost between peak and base flow) resulted in moderate seasonal changes in groundwater  
538 storage (30%) and surface water storage (32%). The EoC simulations reveal larger seasonal  
539 variation for groundwater and surface water storage (40% and 37% decreases, respectively).  
540 Groundwater in the Cosumnes Watershed is mainly recharged in the headwaters and stored in the  
541 Central Valley. Therefore, these Central Valley aquifers experience earlier and larger increases in  
542 storage which lead to more water available to *ET* and therefore aquifer depletion. A deeper  
543 understanding of this phenomenon requires an analysis of the spatial patterns of these changes  
544 which is performed later on in this study.



545

### 546 **3.3.2. Dry water years**

547 All EoC WYs are characterized by higher precipitation in the form of rainfall compared to  
548 their historical counterparts. The historical dry WY has ~43% less total precipitation than the EoC  
549 dry WY. However, we note that for the EoC dry WY the decrease in snowfall is less drastic than  
550 the median or wet EoC years. This is because the historically driest WY is significantly warmer  
551 than the historical average WY, and therefore already has a smaller snowpack, 94% lower than the  
552 historical median WY. The EoC dry WY *SWE* also accumulates two months earlier than the  
553 historical *SWE*. Because the differences in *SWE* between the dry WYs are smaller than the  
554 differences in *SWE* between the median WYs (7% versus 91%), we can deduce that the early and  
555 larger rise in soil moisture in the EoC dry WY is mostly due to an earlier and larger amount of  
556 rainfall. The higher soil moisture and EoC temperatures result in higher *ET* throughout the WY  
557 compared to the historical WY. This *ET* results in lower soil moisture by the end of the summer,  
558 similar to the median WY. In addition, surface water storage peaks earlier and at a larger amount  
559 compared to the historical WY. The surface water storage in the EoC remains higher throughout  
560 the WY compared to its historical counterpart despite this higher *ET* due to the low precipitation  
561 associated with the historical dry WY. We further note that the difference in surface water storage  
562 during baseflow conditions between the two dry WYs is higher than the difference between the  
563 two median WYs. The groundwater recharge starts two months earlier in the EoC driest WY  
564 compared to the historical driest WY due to the changes in timing and magnitude of precipitation.  
565 However, it is interesting to note that groundwater storage during baseflow conditions in the EoC  
566 WY is nearly equal to the historical WY (within 3%). Thus, although more water enters the EoC  
567 dry WY system through greater precipitation, it eventually exits by the end of the WY and no



568 considerable net gains to groundwater are observed. This significant reduction in groundwater  
569 storage from late-winter to end-of-summer is a result of the much larger EoC *ET* and highlights  
570 the dynamic nature of the EoC dry year watershed interactions. Also similar to the median WY,  
571 dry WY seasonal decreases in EoC storage are more pronounced in the groundwater signal (36%)  
572 than in the surface water signal (33%). We further note that the decreases in groundwater and  
573 surface water storages are, as in the median WY, larger (+8%) than the historical decreases.

574

### 575 **3.3.3. Wet water years**

576 The EoC wet WY is significantly wetter than all other WYs. Yet, unlike the historical WY,  
577 the precipitation largely comes as rain, as shown by the low-to-no snowfall and *SWE* totals (Figure  
578 6). The difference in future versus contemporary wet WY *SWE* (99%) is larger than the differences  
579 between the median and the dry WYs (91%). As in other WYs, soil moisture increases earlier  
580 compared to the historical wet WY. A greater water availability enables the system to meet the  
581 high EoC *ET* demand. Hence, *ET* in the EoC wettest year remains higher than the historical wettest  
582 year *ET* throughout the WY. However, the increase in *ET*, combined with the lack of snowmelt  
583 that can buffer and recharge soil moisture in spring, leads to less soil moisture at the end of the  
584 WY compared with the historical WY. Further, surface water storage increases earlier and at a  
585 much faster rate in the EoC WY compared to the historical WY. This is mirrored in the  
586 groundwater storages. As in the other EoC simulations, when compared to the historical  
587 counterpart the EoC wettest year shows a sharper decline in seasonal above and below ground  
588 water storage changes (occurring between peak flow and baseflow). Groundwater storage  
589 decreases 47% in the EoC between peak flow and baseflow, whereas only a 41% decrease occurs



590 in the historical wet WY. Similarly, surface water storage decreases 44% in the EoC whereas only  
591 a 41% decrease occurs in the historical wet WY.

592

### 593 **3.4. Spatial patterns of the changes in fluxes and pressure-heads**

#### 594 **3.4.1. Median water years**

595 To provide a deeper understanding of how the changes in precipitation timing, magnitude,  
596 and phase affect the land surface processes and surface and subsurface hydrodynamic responses,  
597 we assess the spatial patterns of these changes during two key periods in the WY, peak flow and  
598 baseflow. Figure 7 shows the percent changes in *ET*, surface water pressure-heads, and subsurface  
599 pressure-heads (i.e., pressure-heads of the model bottom layer) in the EoC median WY compared  
600 to the historical median WY during peak flow and baseflow conditions (see the time frames in  
601 Figure 6). Regions in red correspond to areas with smaller fluxes or pressure-heads in the EoC  
602 compared to the historical ones, whereas regions in blue correspond to areas with larger fluxes or  
603 pressure-heads in the EoC compared to the historical median WY. We study peak flow and  
604 baseflow conditions because the analysis of the temporal variations of fluxes and storages has  
605 shown that these two periods are characterized by different trends and represent the key periods in  
606 understanding the hydrologic responses to the EoC extreme climate.

607 Relative to the historical median WY, during peak flow the EoC median WY is  
608 characterized by an increased *ET* across the majority of the watershed, especially in the Central  
609 Valley, and larger surface water and subsurface pressure-heads (Figure 7a-c). *ET* increases in the  
610 EoC both because of the increase in water availability and increased evaporative demand, as  
611 discussed in the previous section (3.3.1.). The increase in *ET* is non-uniform across the watershed  
612 because of the heterogeneity of the landscape's topographical gradients, land-surface cover, and



613 subsurface geological conditions. The Central Valley is characterized by a large increase in *ET*  
614 compared to the Sierra Nevada, and the patterns of *ET* in the Central Valley are also more  
615 homogeneous, a resultant of the geological characteristics of the area and the hydroclimate of the  
616 watershed (i.e. where most of the precipitation falls over the Sierra Nevada but follows topographic  
617 gradients downward into the valley where more recharge occurs). This leads to more water  
618 available in the Central Valley compared to the Sierra Nevada characterized by less permeable  
619 rocks. In addition, as most of the *ET* in the Central Valley comes from evaporation due to the high  
620 temperatures of the EoC (not shown here), the increase in evaporation is higher in the Central  
621 Valley due to its aquifers characterized by a high permeability (Maina and Siirila-Woodburn,  
622 2020) and the availability of water.

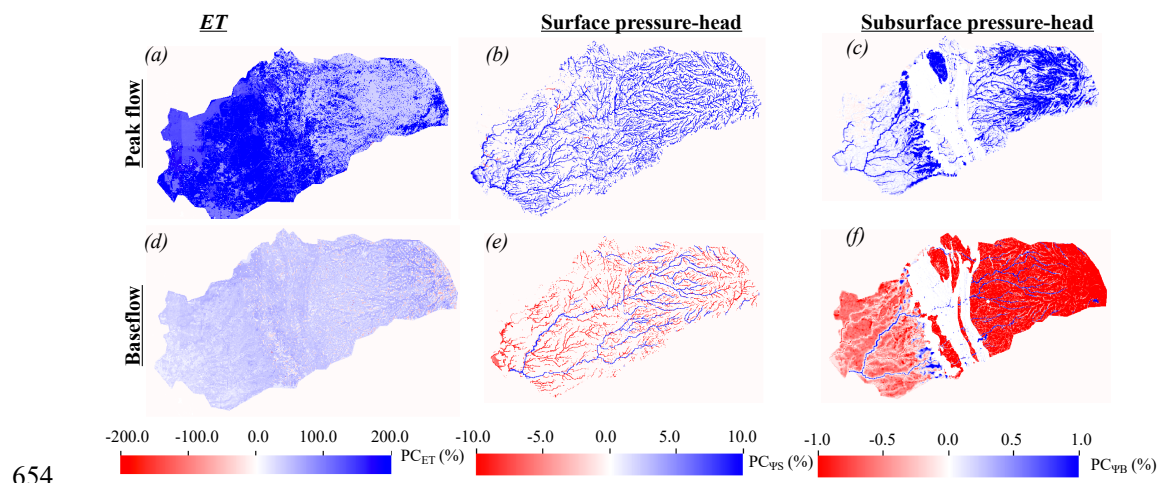
623         Surface and subsurface pressure heads both show general increases during the EoC peak  
624 flow, yet these maps reveal that unlike *ET* the pressure head (and therefore storage) of water is  
625 very heterogeneous in space. For example, in the Sierra Nevada, we observe an increase in  
626 subsurface pressure-head (Figure 7c) only in some relatively permeable areas susceptible to  
627 infiltration and recharge. Although the Central Valley aquifers are more permeable and  
628 geologically less heterogeneous than the Sierra Nevada (as defined in the model), the changes in  
629 subsurface pressure-head in the Central Valley are heterogeneous. This is because the recharge of  
630 the Central Valley aquifers is dependent on the subsurface and surface flows from the headwater  
631 (i.e., connectivity to the headwater). In other words, only areas of the Central Valley that are  
632 subject to stronger connectivity with the headwaters see an increase in subsurface pressure-head  
633 in the EoC, likely because they are more regularly recharged by the headwaters through surface  
634 and subsurface flows from these areas, a recharge that buffers the water depletion through *ET*.





635 These are mostly the areas located close to the streams where there is an exchange between the  
636 subsurface and the surface and the Sierra Nevada foothills (in the alluvium 3 area, see Figure 1).

637 Relative to its historical counterpart, the EoC median WY is characterized by high *ET*  
638 during baseflow conditions though less than during peak flow conditions. (Figure 7d). We observe  
639 larger surface water pressure-heads in higher-order streams whereas surface water pressure-heads  
640 decrease in the EoC in the majority of the low-order, ephemeral streams (Figure 7e). This  
641 opposition of spatial pattern trends, resulting in more water in the main river channels, and less in  
642 the smaller streams, occurs for several reasons. First, peak flow occurs earlier in the EoC and is  
643 more rainfed, so that the ephemeral streams drain earlier in the EoC compared to in the historical  
644 period. This sustained and longer duration of draining increases the surface water pressure-head  
645 along the main river channels and is due to the contribution of the subsurface in the headwaters.  
646 This contribution is also higher in the EoC due to larger amounts of precipitation. The trends along  
647 the main river channel are also evident in the subsurface pressure-head maps (Figure 7f). Because  
648 the surface water is larger along the main channels, the subsurface pressure-heads are also larger  
649 here due to the interconnection between the subsurface and the surface (Figure 7f). However, in  
650 general, subsurface pressure-heads decrease elsewhere in the EoC during baseflow because of the  
651 lack of snowmelt and the higher *ET* demand. This result highlights the spatiotemporal complexity  
652 of an expected watershed's response to changes in climate (shown here to be bi-directional), and  
653 how factors such as river proximity may be crucial for consideration.



654

655 Figure 7: Comparisons between EoC median water year (WY) and the historical median WY peak  
656 flow and baseflow spatial distributions of percent changes in  $ET$  ( $PC_{ET}$ ), surface water ( $PC_{\psi_S}$ ) and  
657 subsurface ( $PC_{\psi_B}$ ) pressure-heads. Regions in red correspond to areas with smaller fluxes or  
658 pressure-heads in the EoC compared to the historical ones, whereas regions in blue correspond to  
659 areas with larger fluxes or pressure-heads in the EoC compared to the historical WY.

660

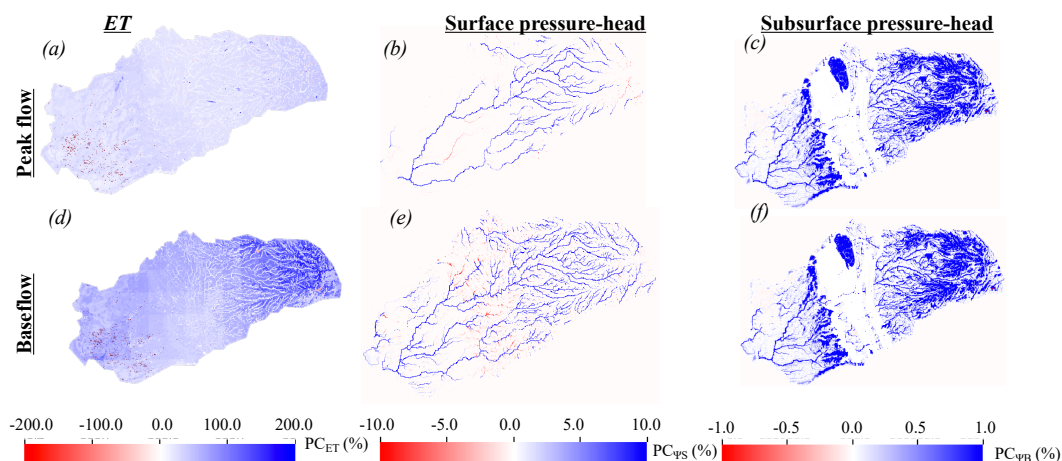
### 661 3.4.2. Dry water years

662 Figure 8 illustrates the percent changes in  $ET$ , surface water, and subsurface pressure-heads  
663 in the EoC dry WY compared to the historical dry WY during peak flow and baseflow conditions.  
664 During peak flow conditions, the EoC dry WY has larger  $ET$ , surface, and subsurface pressure-  
665 heads than the historical dry WY (Figure 8a-c).  $ET$  is larger in this EoC dry WY not only because  
666 it is hotter, but also because there is more precipitation, as noted previously. Increases in surface  
667 pressure-heads are non-uniform across the domain. For example, surface water does not increase  
668 in high elevation areas (i.e. elevation > 2000m) in the EoC dry WY because the change in the  
669 precipitation phase is not significant. The main difference between the EoC and the historical dry



670 WY is the amount of the water flowing down gradient, which is higher in the EoC, hence the  
671 surface water in the EoC becomes higher downstream. The increase in subsurface pressure-heads  
672 in the EoC dry WY during peak flow conditions is heterogeneous with patterns similar to the  
673 changes in subsurface pressure-heads associated with the EoC median WY.

674 During baseflow conditions, even though *ET* increases in the EoC driest WY relative to  
675 the historical driest WY, surface, and subsurface pressure-heads also generally increase (Figure  
676 8d-f). Given wetter conditions in the driest EoC WY, first-order streams are more pronounced. A  
677 few low-order streams have less surface water in the EoC when compared to the historical dry  
678 WY, similar to the results of the median WYs (see section 3.4.2). Subsurface pressure-head is  
679 generally larger in areas subject to strong connectivity with the headwaters (i.e., receiving more  
680 water from the headwaters through subsurface and surface flows) in the EoC dry WY relative to  
681 the historical dry WY, with some regions experiencing no change from the historical conditions.  
682 This suggests that the larger amount of precipitation associated with the EoC dry WY is sufficient  
683 to supply enough water to account for high *ET* demands and recharge the groundwater.



684  
685 Figure 8: Comparisons between EoC dry water year (WY) and the historical dry WY peak flow  
686 and baseflow spatial distributions of percent changes in *ET* ( $PC_{ET}$ ), surface water ( $PC_{PS}$ ) and

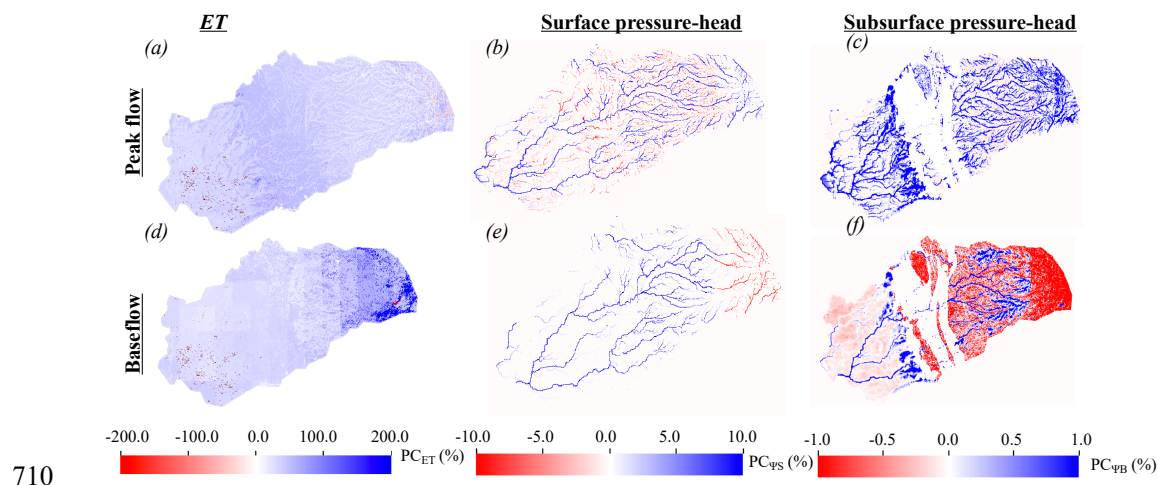


687 subsurface ( $PC_{\psi_B}$ ) pressure-heads. Regions in red correspond to areas with smaller fluxes or  
688 pressure-heads in the EoC compared to the historical ones, whereas regions in blue correspond to  
689 areas with larger fluxes or pressure-heads in the EoC compared to the historical WY.

690

### 691 **3.4.3. Wet water years**

692 Figure 9 shows the percent changes in  $ET$ , surface water, and subsurface pressure-heads in  
693 the EoC wet WY compared to the historical wet WY during peak flow and baseflow conditions.  
694 During peak flow, the EoC wet WY is characterized by larger  $ET$  and subsurface pressure-heads  
695 relative to the historical wet WY and a more heterogeneous mixture of regions with both higher  
696 and lower surface water conditions throughout the catchment (Figure 9 a-c). Analogous to other  
697 WYs at EoC, the surface water pressure-head increases (decreases) are apparent in larger-order  
698 (smaller order) streams, both in the Sierra Nevada and in the Central Valley. In the wettest WY,  
699 this occurs for several reasons. First, the larger volume of precipitation, plus seasonal shifts in  
700 precipitation timing result in the filling of the higher-order streams and depletion of the lower-  
701 order streams during peak flow. Second, in the historical wet WY, a significantly greater amount  
702 of snowpack is present in the Sierra Nevada in the upper elevation of the headwaters, allowing for  
703 slower, steadier amounts of water that is released during the spring via snowmelt, and in turn,  
704 supporting low-order streams over a longer period of time. The latter effect is immediately visible  
705 in Figure 9e, where decreases in EoC surface pressure heads are visible in the headwaters, despite  
706 the watershed-total showing an increase in EoC surface water storage during baseflow (see Figure  
707 6). Similar to the two previous EoC WYs, the subsurface pressure-head increases are shown more  
708 distinctly in the Central Valley during peak flow, under the main river channels, and in the foothills  
709 during baseflow (see previous sections on the discussion of hydroclimatic and geologic impacts).



710

711 Figure 9: Comparisons between EoC wet water year (WY) and the historical wet WY peak flow  
712 and baseflow spatial distributions of percent changes in  $ET$  ( $PC_{ET}$ ), surface water ( $PC_{\psi_S}$ ) and  
713 subsurface ( $PC_{\psi_B}$ ) pressure-heads. Regions in red correspond to areas with smaller fluxes or  
714 pressure-heads in the EoC compared to the historical ones, whereas regions in blue correspond to  
715 areas with larger fluxes or pressure-heads in the EoC compared to the historical WY.

716

#### 717 4. Discussion

##### 718 4.1 Comparison with previous studies

719 Some of the results presented in this study are qualitatively in agreement with previous  
720 studies yet provide important new insights. For example, Maurer & Duffy, (2005) used 10 global  
721 climate models to predict, as in this study, an increase in winter flows with an earlier peak flow  
722 timing in the WY and a decrease in summer flows. Maurer & Duffy show that mid-century  
723 projected annual precipitation and streamflow increases of 7% and 13% (respectively). Although  
724 our study focused on EoC projections, we found that compared to the historical median WY,  
725 annual surface water will increase by 19% in the EoC median WY. Compared to their findings,



726 our work sheds light on how these changes in runoff will occur across the watershed based on its  
727 physical characteristics and highlights that while runoff will increase in the EoC lower-order  
728 streams mainly located in the Sierra Nevada will see a decrease due to the change in the  
729 precipitation phase. Mallakpour et al., (2018) also had a similar finding in a study that shows that  
730 future California streamflow is altered similarly to Maurer & Duffy, (2005) under both the RCP4.5  
731 and RCP8.5 emissions scenarios, with RCP8.5 showing the highest changes during peak flow.  
732 However, contrary to our work the authors mentioned that the annual changes in streamflow will  
733 not be significant probably due to the compensation between increases in peak flow and decreases  
734 in baseflow. This was likely shaped by the differences in climate and hydrologic models used to  
735 derive these conclusions. Similar changes in streamflow were obtained by He et al., (2019) who  
736 drove the hydrologic model VIC with 10 global climate models to understand potential changes in  
737 runoff in California due to climate change. Hydrologic changes computed from the 10 global  
738 climate models were consistent and robust and showed an increase of around 10% in annual  
739 streamflow by the late century, a percentage similar to what has been found in this study. The  
740 authors mentioned that watershed characteristics such as geology, topography, and land cover  
741 strongly impact the hydrologic response to climate change. Relationships between watershed  
742 characteristics (e.g., physiographic parameters) and its responses to climate change were further  
743 explored by Son & Tague, (2019) who highlighted that because vegetation and subsurface geology  
744 control both water availability and energy demand, they in turn influence watershed sensitivity to  
745 a changing climate as shown in this study.

746         The increases in groundwater storage shown in this study are also in agreement with  
747 Niraula et al., (2017) who used the hydrologic model VIC to show that groundwater recharge will  
748 likely increase in the northern portion of the western United States in a changing climate. However,



749 contrary to their work that estimates changes in groundwater recharge over a large domain (i.e. the  
750 western United States). In this work, we show that groundwater recharge decreases in the summer  
751 in some areas due to the lack of snowmelt and high EoC *ET*. Increases in *ET* in response to global  
752 warming were also documented by Pascolini-Campbell et al., (2021) who showed a 10% increase  
753 in global *ET* from 2003 to 2019.

754 An advantage of our approach is a more explicit estimate of spatiotemporal changes in  
755 groundwater-surface water feedbacks because Parflow-CLM physically solves the transfer and  
756 movement of water from the bedrock to the canopy. Additionally, the aforementioned studies used  
757 different emission scenarios and models to project changes in hydrology, nonetheless, their results  
758 have shown that the directions of the observed changes are consistent across models and emission  
759 scenarios and only the magnitude of these changes is uncertain. Hence, the trends observed in this  
760 study using a single model and emission scenario likely represent the trends we would observe  
761 using different models and scenarios. While our results show similar patterns and changes, our  
762 study provides a much finer-grained perspective on the sensitivity of a watershed to changes in  
763 climate extremes based on its subsurface geology, topography, and land cover. It also highlights  
764 that the spatiotemporal analyses of these changes may reveal different trends than if only assessed  
765 as annual changes. Understanding these localized changes and sensitivities is critical and has  
766 practical implications for water management.

767

#### 768 **4.2 Implications for water resources management**

769 Because our work provides a better understanding of the spatiotemporal changes in  
770 hydrodynamics in response to future extremes, our findings also have important implications for  
771 water resources in California. While previous work more broadly focused on how temperature



772 increases will alter the precipitation phase and reduce seasonal snowpack and increase winter  
773 runoff, this work brings new physical and more granular insights into how watersheds may respond  
774 to climate extremes. In particular, both wet and dry WYs in the future experience increased  
775 precipitation. As such, even in future dry WYs, water managers and stakeholders may need to  
776 prepare more for large precipitation events that may increase the possibility of flooding and require  
777 new infrastructure management strategies. For example, in a future where WYs are generally  
778 wetter, having alternatives for water supply during periods of sustained drought could be less  
779 important. However, as we show in this paper, shifts in precipitation timing, phase, and magnitude  
780 have cascading impacts on soil moisture profiles and *ET* withdrawals, which subsequently impact  
781 discharge and groundwater dynamics. Future shifts in water availability earlier in the year, as well  
782 as more dynamic transitions between peak and baseflow conditions (as quantified here), may  
783 impose stresses on water distribution, especially those systems already under scrutiny (e.g. those  
784 resources over-allocated or facing environmental degradation).

785         In addition, while these projections show increases in surface water and groundwater  
786 storages at watershed-scale, our results also highlight important localized spatiotemporal changes  
787 across a watershed, where the assumption of water storage increase does not necessarily hold in  
788 all geographic locations (e.g., areas that are not close to the river in the Central Valley). Our study  
789 also shows that the decreases in groundwater storage in the Central Valley aquifers are more  
790 significant than the decreases in surface water storage during baseflow conditions. This may call  
791 for new conveyance infrastructure that can move water from the relatively wetter areas to the drier  
792 areas and/or where infiltration can more readily occur. The latter suggests solutions such as  
793 Managed Aquifer Recharge (MAR) could become an increasingly important climate change  
794 adaptation. Finally, our study also highlights that lower-order streams will likely become more





795 ephemeral in the EoC due to flashier runoff and higher evaporative demand, such conditions will  
796 have important implications for fish spawning and ecosystem nutrient cycling. Although our  
797 results are embedded with uncertainties and are based on a single projection and model, they do  
798 highlight the need for a revisitation of current water management strategies. Further studies using  
799 different climate and land-use scenarios and models of varying complexity and resolution could  
800 help build more confidence and provide more information in defining how future water  
801 management strategies would need to change to be more resilient to more extreme WYs in the  
802 future.

803

#### 804 **4.3 Study limitations**

805 This study combines novel climate and hydrologic simulations that provide both  
806 advantages and disadvantages compared with previous work (He et al., 2019; Maurer & Duffy,  
807 2005; Niraula et al., 2017; M. Safeeq et al., 2014; Son & Tague, 2019). We note several of these  
808 disadvantages below. In the integrated hydrologic model, the subsurface geology and land cover  
809 characterization has inherent and, in some cases, irreducible uncertainty. This study uses  
810 hydrodynamic parameters as defined by Maina et al. (2020a), which assumes that the subsurface  
811 hydrodynamics from the Sierra Nevada to the Central Valley is almost completely hydrologically  
812 separated except through overland flow. However, it is not clear whether fractures or other  
813 macrostructures may drive more surface and subsurface flows from the headwaters to the Central  
814 Valley aquifers. In addition, we use the historical land surface cover map when simulating the  
815 EoC. Since vegetation will dynamically respond to a changing climate, the land surface cover used  
816 in the EoC simulations may be unrealistic and may influence, for example, *ET* and/or soil moisture.  
817 For example, it has been shown that the stomatal resistance of plants will change due to rising CO<sub>2</sub>



818 with important implications for both the water and energy balance (Lemordant et al., 2018; Milly  
819 & Dunne, 2017). Yet, our use of historical land surface cover does have the advantage of isolating  
820 changes in fluxes associated with climate change alone and could be compared in future work with  
821 additional simulations that account for both changes in the land surface and climate. Future studies  
822 will assess the impact of changes in vegetation physiology and land surface cover on watershed  
823 hydrodynamics. In this study, we did not include the impacts of anthropogenic activities such as  
824 pumping and irrigation due to the uncertainties in predicting these fluxes in EoC. While these  
825 human interventions could substantially change the hydrologic system, our study isolates the  
826 impacts of a changing climate on the natural system. Future studies can now estimate the impacts  
827 of different pumping and irrigation scenarios at EoC that may further impact the hydrologic system  
828 hydrodynamics in a changing climate and compare and contrast with this work. Last, although our  
829 VR-CESM simulations represent a cutting-edge global climate model simulation (e.g., 28 km  
830 regional grid-refinement, coupled atmosphere-land simulation with prescribed ocean conditions,  
831 etc.), further work may be needed to evaluate how a more refined grid resolution impacts  
832 atmospheric process representation over the Cosumnes watershed, particularly in the headwaters  
833 (Maina et al., 2020b). We further acknowledge that the 30-year simulation may not be sufficient  
834 to capture certain climate extremes (e.g., 1-in-50-year storm). Future studies, if computational  
835 resources are available, will seek to explore how the use of a longer time period might influence  
836 the identification of the most extreme dry and wet WYs from VR-CESM.

837

## 838 **5 Summary and Conclusions**

839 The effects of climate change are increasingly felt across many regions of the world,  
840 especially in hydrologically sensitive regions with Mediterranean climates such as California.



841 Many studies over the years have been conducted to better understand the hydroclimate of the EoC  
842 and its impacts on the hydrologic cycle. Previous studies have used a multitude of different models  
843 at varying complexity and climate scenarios to highlight that the future climate has multiple  
844 plausible outcomes. Most of these studies indicate warmer temperatures and precipitation that  
845 mostly falls as rain instead of snow. For example, the state of California is projected to experience  
846 more punctuated climate extremes coupled with a marked decrease in the Sierra Nevada snowpack  
847 (Cayan et al., 2008; Gleick, 1987; Musselman, Molotch, et al., 2017; Rhoades, Ullrich, &  
848 Zarzycki, 2018). Such drastic transitions have already started to shape the hydroclimate of  
849 California. Faced with this new normal, it is becoming increasingly important to assess how the  
850 integrated hydrologic cycle may respond to these perturbations and connect these responses more  
851 directly to water resource management, particularly with modeling frameworks that can better  
852 represent the interactions between the changing atmosphere and the surface and subsurface  
853 hydrology.

854 In this work, we used state-of-the-art physics-based models at high resolutions for their  
855 respective communities to project changes in meteorological conditions at the EoC and assess how  
856 their combined effects influence watershed hydrology from the land surface to the deeper  
857 subsurface. Importantly, our approach to couple a variable resolution Earth System Model and an  
858 integrated hydrologic model allow for us to simulate hydro-meteorological conditions which are  
859 jointly driven by thermodynamical and dynamical shifts in climate. We model the Cosumnes  
860 watershed, which spans the Sierra Nevada and Central Valley and hosts one of the last rivers in  
861 the state without a large dam, as a testbed to understand how climate drivers will impact water  
862 resources in the EoC. We performed climate simulations over 30-year periods historically (1985-  
863 2015) and at EoC (2070-2100) and identified the driest, median, and wettest WYs from those



864 simulations, which were then used as meteorological forcing for the hydrologic model. Our  
865 coupled simulations project that, for the Cosumnes watershed, temperature and precipitation will  
866 both increase by the EoC across all WY types (wettest, median, and driest). In addition,  
867 precipitation is projected to fall earlier compared to historical conditions and mainly in the form  
868 of rain. For the median and wet WYs the precipitation season has earlier cessation dates, while the  
869 dry EoC WY, which is wetter than its historical counterpart, persists significantly longer into the  
870 spring. As a consequence of warmer temperatures, all WYs show a substantial decrease in *SWE*.  
871 The shift of precipitation from snowfall to rainfall, as well as the increase in the amount of  
872 precipitation and the early start of precipitation lead to an overall increase in soil moisture and  
873 more water available to meet the higher EoC *ET* demand. Importantly, this increase in *ET* is  
874 heterogeneous across the watershed and highlights one of the main advantages of using an  
875 integrated hydrologic model such as the one we employed in this study to assess the spatiotemporal  
876 patterns of change. Our results show that the sensitivity to the changes in *ET* at EoC depends on  
877 the subsurface geology and topographical gradients. More specifically:

- 878 • The geological and topographical complexities of the Sierra Nevada headwaters  
879 lead to highly heterogeneous changes in *ET*. Changes in *ET* are higher in permeable  
880 areas such as the plutonic rocks where water can be more easily extracted.
- 881 • *ET* changes in the Central Valley of the Cosumnes watershed are predominantly  
882 uniform with the highest sensitivities in the vicinity of the Cosumnes River due to  
883 the high availability of water.

884 Precipitation increases enough in the EoC to provide water for both increased *ET* and  
885 increased surface water storage. Surface water storages also increase earlier in the WY and have  
886 higher peak amounts. This earlier and larger increase is a direct consequence of an earlier start in



887 precipitation at EoC, a marked change in the precipitation phase, and an overall larger amount of  
888 precipitation when compared with the historical WYs. However, our results also highlight that  
889 during baseflow conditions surface water decreases, especially in lower-order streams, showing  
890 that these areas are highly sensitive to the change in precipitation phase. Our simulations also show  
891 that the seasonal variability of the EoC watershed behavior is also more dynamic. In general,  
892 decreases in seasonal water storages occurring between peak flow and baseflow conditions are  
893 more than 10% higher in the EoC compared to the historical conditions.

894 EoC groundwater storages are also projected to increase earlier in the WY with peaks  
895 greater than those found historically. Yet these storages decrease significantly during baseflow  
896 conditions due to the higher *ET* at EoC and the absence of recharge from snowmelt. Contrary to  
897 the changes in surface water storages, groundwater storages show a larger decrease due to their  
898 dependence on the surface water from the Sierra Nevada. Our results also show that changes in  
899 subsurface pressure-heads are not uniform and are bi-directional throughout the Cosumnes  
900 watershed. Because the connectivity between the Central Valley aquifers and the Sierra Nevada  
901 headwaters (i.e., subsurface and surface flows from the headwater to the Central Valley aquifers)  
902 plays an important role in the hydrodynamics of this watershed, only areas with a strong connection  
903 with the headwaters, such as the foothills and the river channels, see an increase in subsurface  
904 pressure-heads at EoC. However, the subsurface pressure-heads decrease elsewhere in the Central  
905 Valley aquifers especially in baseflow conditions due to the high *ET* and the lack of snowmelt. In  
906 the river channels, this is due to the exchange between the subsurface and the surface whereas the  
907 foothills characterized by the consolidated sediments serve as “spillover.”

908 Our results provide novel understandings about possible changes in the integrated  
909 hydrologic response to changes in EoC climate extremes. An important caveat is that our



910 simulation was a single set of climate realizations and may not properly bound internal variability  
911 uncertainty like an ensemble of climate simulations could. However, beyond the widely agreed-  
912 upon changes of decreased snowpack and shifts in runoff timing in the literature, we show that in  
913 this simulation: 1) EoC precipitation increases even in the driest years; 2) despite increased  
914 temperature, and hence ET, both groundwater and surface water storage increase relative to  
915 historical conditions because of increased precipitation; and 3) there is a distinct spatial pattern,  
916 particularly in surface water storage, in which smaller-order streams see reduced flow while the  
917 larger order streams see increased flow. These changes will have strong implications on natural  
918 resource management.

919 In this study, land cover changes are assumed to not occur, however, changes in land cover  
920 are expected to occur in the future, either naturally or anthropogenically. Further vegetation  
921 physiology will also change in response to an increase in CO<sub>2</sub>. Thus, future studies should  
922 investigate the impacts of these changes and how they may further alter the integrated hydrologic  
923 budgets. Additionally, future studies could also assess the effects of anthropogenic activities such  
924 as pumping and irrigation under a changing climate, other emissions scenarios, and/or the  
925 sequencing of variable end-member WYs and the interannual memory of the hydrologic system.  
926 Importantly, an understanding of this variability could be used to inform how water managers  
927 might prepare for more intense and/or intermittent extremes in the future. Future research could  
928 also use multiple emission scenarios to better assess the range in hydrodynamic responses  
929 dependent on the severity of climate change, especially those related to the magnitude and spatial  
930 location of the precipitation response since they are likely more uncertain and scenario-dependent  
931 than the trends at the watershed-scale.

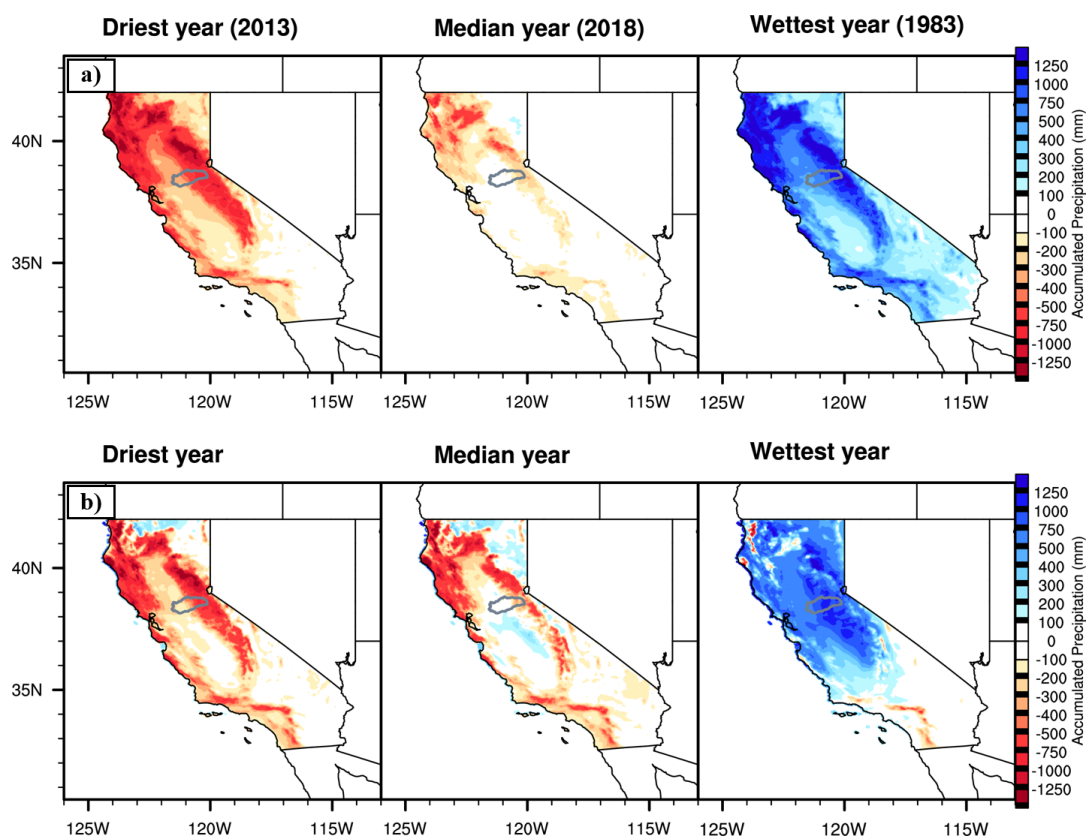


932 **Appendix A: Comparisons between VR-CESM and PRISM historical conditions**

933 Figure A1 highlights differences in dry, median, and wet WY accumulated precipitation  
934 relative to the 1981-2019 PRISM climatology. VR-CESM generally recreates the spatial pattern  
935 of anomalous dry and wet patterns across California for each WY type. This is shown via the  
936 common regions of minimum and maximum anomalies relative to the PRISM climatology.  
937 Notably, there are regions where VR-CESM anomalies are not consistent with PRISM. This is  
938 primarily shown in the wettest water year in portions of the Central Valley, western slopes of the  
939 Sierra Nevada, and southern California. This is likely correlated with resolution and the lack of  
940 orographic gradients (both valleys and peaks) in VR-CESM at 28km resolution. Mismatches in  
941 accumulated precipitation may also be due to representation of atmospheric rivers (ARs) in VR-  
942 CESM that were found to be generally larger, slightly more long-lived and make landfall more  
943 frequently over California (Rhoades et al., 2020b). Figure A2 shows Cosumnes watershed WY  
944 accumulated precipitation and surface temperature. WY accumulated precipitation is shown in  
945 Figure A 2a and 2b for PRISM and VR-CESM, respectively. All WY accumulated precipitation  
946 simulated by VR-CESM over 1985-2015 are within the range in PRISM, save for the wettest WY.  
947 This is shown more explicitly in quadrant space in Figure A2c where the range of annual bias in  
948 VR-CESM relative to the range of interannual variability in PRISM for accumulated precipitation  
949 and temperature is shown. VR-CESM generally simulates a wetter historical period over the  
950 Cosumnes (range of bias of 1330 mm) relative to PRISM (range of interannual variability of 1320  
951 mm). Basin-average minimum (421 mm) and maximum (1740 mm) WY accumulated  
952 precipitation are slightly larger than is found in PRISM. Of relevance to this study, PRISM has  
953 shown notable uncertainties in the Sierra Nevada. Lundquist et al., 2015 showed that an  
954 underrepresentation of the most extreme storm total precipitation in the Sierra Nevada can result



955 in an upper-bound uncertainty of 20% in WY accumulated precipitation. Therefore, the wettest  
956 WY of VR-CESM is well within the 20% uncertainty range of PRISM's wettest WY ( $1580 \pm 316$   
957 mm). Further, differences in basin-average WY accumulated precipitation between VR-CESM  
958 and PRISM are non-significant using a t-test and assuming a p-value  $< 0.05$ . The range of  
959 temperature bias in VR-CESM ( $2.74\text{ }^{\circ}\text{C}$ ) relative to the range of PRISM interannual variability  
960 ( $2.93\text{ }^{\circ}\text{C}$ ) was also within the temperature uncertainties discussed in Strachan and Daly, 2017.  
961 They showed that a general cool-bias in PRISM temperatures were found on the leeward side of the  
962 Sierra Nevada when compared with 16 out-of-sample in-situ observations across an elevation  
963 gradient of 1950 to 3100 meters with an overall mean bias of  $-1.95\text{ }^{\circ}\text{C}$  (maximum temperature)  
964 and  $-0.75\text{ }^{\circ}\text{C}$  (minimum temperature).

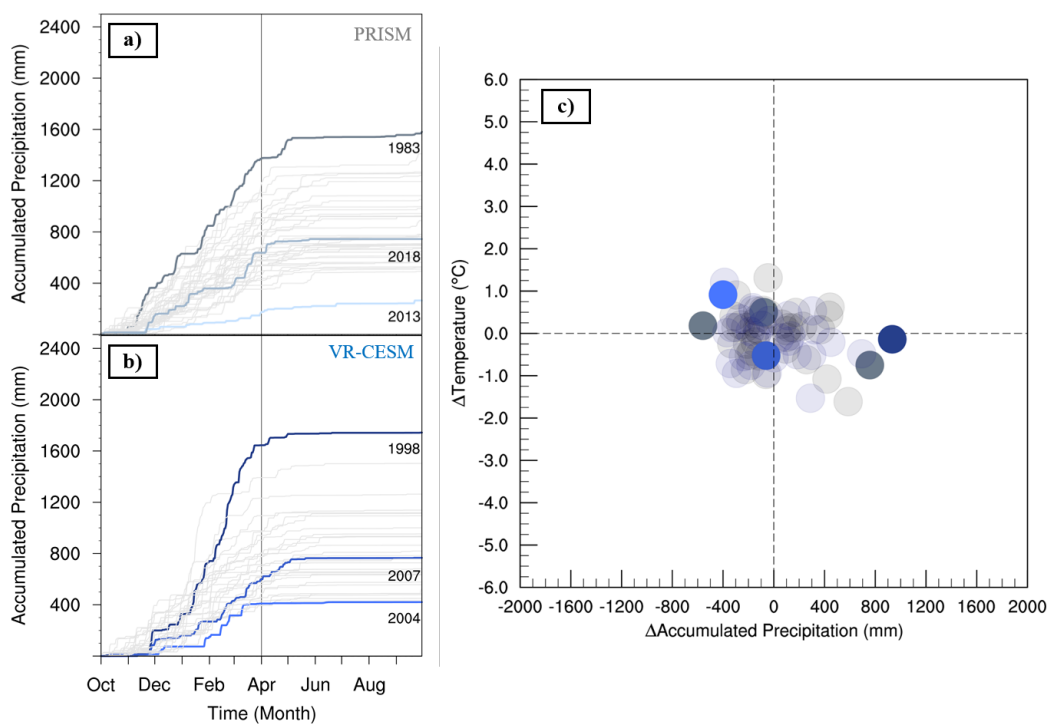


965





966 Figure A1: Differences in the driest, median, and wettest water year accumulated precipitation  
967 over California in a) PRISM and b) VR-CESM relative to the 1981-2019 PRISM climatology.  
968 The Cosumnes watershed boundary is outlined in gray.



969  
970 Figure A2: Cosumnes watershed accumulated precipitation totals in a) PRISM (gray; 1981-2019)  
971 and b) VR-CESM (blue; 1985-2015) with dry, median, and wet years emboldened. c) shows  
972 differences in PRISM (gray) and VR-CESM (blue) relative to the PRISM climatology (1981-2019)  
973 in temperature and accumulated precipitation quadrant space. Dry, median, and wet water years  
974 are emboldened.

#### 975 Data availability

976 Data supporting the findings of this study can be found here:  
977 <https://portal.nersc.gov/archive/home/a/arhoades/Shared/www/Hyperion/>



978 **Author contribution**

979 The authors contribute equally to this work.

980 **Competing interests**

981 The authors declare that they have no conflict of interest.

982 **Acknowledgements**

983 Fadji Zaoua Maina and Erica Siirila-Woodburn were supported by LDRD funding from Berkeley  
984 Lab, provided by the Director, Office of Science, of the U.S. Department of Energy under Contract  
985 No. DE-AC02-05CH11231.

986 Author Alan M. Rhoades was funded by the Department of Energy, Office of Science Office of  
987 Biological and Environmental Research program under Award Number DE-SC0016605 "A  
988 framework for improving analysis and modeling of Earth system and intersectoral dynamics at  
989 regional scales" and Award Number DE-AC02-05CH11231 "The Calibrated and Systematic  
990 Characterization, Attribution, and Detection of Extremes - Science Focus Area".

991 This research used computing resources from the National Energy Research Scientific

992 Computing Center, a DOE Office of Science User Facility supported by the <http://>

993 [dx.doi.org/10.13039/100006132](http://dx.doi.org/10.13039/100006132) of the U.S. Department of Energy under Contract No. DE-

994 AC02-05CH11231.

995



996

997

## References

- 998 Allan, R.P., Barlow, M., Byrne, M.P., Cherchi, A., Douville, H., Fowler, H.J., Gan, T.Y.,  
999 Pendergrass, A.G., Rosenfeld, D., Swann, A.L.S., Wilcox, L.J. and Zolina, O. (2020),  
1000 Advances in understanding large-scale responses of the water cycle to climate change.  
1001 Ann. N.Y. Acad. Sci., 1472: 49-75. <https://doi.org/10.1111/nyas.14337>
- 1002 Alo, C. A., & Wang, G. (2008). Hydrological impact of the potential future vegetation response to  
1003 climate changes projected by 8 GCMs. *Journal of Geophysical Research: Biogeosciences*,  
1004 113(G3). <https://doi.org/10.1029/2007JG000598>
- 1005 Bales, R. C., Molotch, N. P., Painter, T. H., Dettinger, M. D., Rice, R., & Dozier, J. (2006).  
1006 Mountain hydrology of the western United States. *Water Resources Research*, 42(8).  
1007 <https://doi.org/10.1029/2005WR004387>
- 1008 Barnett, T. P., Adam, J. C., & Lettenmaier, D. P. (2005). Potential impacts of a warming climate  
1009 on water availability in snow-dominated regions. *Nature*, 438(7066), 303–309.  
1010 <https://doi.org/10.1038/nature04141>
- 1011 Berghuijs, W. R., Woods, R. A., & Hrachowitz, M. (2014). A precipitation shift from snow  
1012 towards rain leads to a decrease in streamflow. *Nature Climate Change*, 4(7), 583–586.  
1013 <https://doi.org/10.1038/nclimate2246>
- 1014 Cayan, D. R., Maurer, E. P., Dettinger, M. D., Tyree, M., & Hayhoe, K. (2008). Climate change  
1015 scenarios for the California region. *Climatic Change*, 87(1), 21–42.  
1016 <https://doi.org/10.1007/s10584-007-9377-6>
- 1017 Christensen, L., Tague, C. L., & Baron, J. S. (2008). Spatial patterns of simulated transpiration  
1018 response to climate variability in a snow dominated mountain ecosystem. *Hydrological*  
1019 *Processes*, 22(18), 3576–3588. <https://doi.org/10.1002/hyp.6961>



- 1020 Collins, W. D., Bitz, C. M., Blackmon, M. L., Bonan, G. B., Bretherton, C. S., Carton, J. A., et al.  
1021 (2006). The Community Climate System Model Version 3 (CCSM3). *Journal of Climate*,  
1022 *19*(11), 2122–2143. <https://doi.org/10.1175/JCLI3761.1>
- 1023 Condon, L. E., Maxwell, R. M., & Gangopadhyay, S. (2013). The impact of subsurface  
1024 conceptualization on land energy fluxes. *Advances in Water Resources*, *60*, 188–203.  
1025 <https://doi.org/10.1016/j.advwatres.2013.08.001>
- 1026 Condon, L.E., Atchley, A.L., Maxwell, R.M., (2020). Evapotranspiration depletes groundwater  
1027 under warming over the contiguous United States. *Nature Communications* *11*, 873.  
1028 <https://doi.org/10.1038/s41467-020-14688-0>
- 1029 Cook, E. R., Woodhouse, C. A., Eakin, C. M., Meko, D. M., & Stahle, D. W. (2004). Long-Term  
1030 Aridity Changes in the Western United States. *Science*, *306*(5698), 1015–1018.  
1031 <https://doi.org/10.1126/science.1102586>
- 1032 Cosgrove, B. A., Lohmann, D., Mitchell, K. E., Houser, P. R., Wood, E. F., Schaake, J. C., et al.  
1033 (2003). Real-time and retrospective forcing in the North American Land Data Assimilation  
1034 System (NLDAS) project. *Journal of Geophysical Research: Atmospheres*, *108*(D22).  
1035 <https://doi.org/10.1029/2002JD003118>
- 1036 Cristea, N. C., Lundquist, J. D., Loheide, S. P., Lowry, C. S., & Moore, C. E. (2014). Modelling  
1037 how vegetation cover affects climate change impacts on streamflow timing and magnitude  
1038 in the snowmelt-dominated upper Tuolumne Basin, Sierra Nevada. *Hydrological*  
1039 *Processes*, *28*(12), 3896–3918. <https://doi.org/10.1002/hyp.9909>
- 1040 Daly, C., Halbleib, M., Smith, J. I., Gibson, W. P., Doggett, M. K., Taylor, G. H., et al. (2008).  
1041 Physiographically sensitive mapping of climatological temperature and precipitation across the



- 1042 conterminous United States. *International Journal of Climatology*, 28(15), 2031–2064.  
1043 <https://doi.org/10.1002/joc.1688>.
- 1044 Dettinger, M. (2011). Climate Change, Atmospheric Rivers, and Floods in California – A  
1045 Multimodel Analysis of Storm Frequency and Magnitude Changes1. *JAWRA Journal of*  
1046 *the American Water Resources Association*, 47(3), 514–523.  
1047 <https://doi.org/10.1111/j.1752-1688.2011.00546.x>
- 1048 Dettinger, M., & Anderson, M. L. (2015). Storage in California’s reservoirs and snowpack in this  
1049 time of drought. *San Francisco Estuary and Watershed Science*, 13(2).  
1050 <https://doi.org/10.15447/sfews.2015v13iss2art1>
- 1051 Dettinger, M., Redmond, K., & Cayan, D. (2004). Winter Orographic Precipitation Ratios in the  
1052 Sierra Nevada—Large-Scale Atmospheric Circulations and Hydrologic Consequences.  
1053 *Journal of Hydrometeorology*, 5(6), 1102–1116. <https://doi.org/10.1175/JHM-390.1>
- 1054 Dettinger, M. D. (2013). Atmospheric Rivers as Drought Busters on the U.S. West Coast. *Journal*  
1055 *of Hydrometeorology*, 14(6), 1721–1732. <https://doi.org/10.1175/JHM-D-13-02.1>
- 1056 Di Liberto, T. (2017, October). Very wet 2017 WY ends in California. *NOAA Climate.Gov*.  
1057 Retrieved from [https://www.climate.gov/news-features/featured-images/very-wet-2017-](https://www.climate.gov/news-features/featured-images/very-wet-2017-water-year-ends-california)  
1058 [water-year-ends-california](https://www.climate.gov/news-features/featured-images/very-wet-2017-water-year-ends-california)
- 1059 Dierauer, J. R., Whitfield, P. H., & Allen, D. M. (2018). Climate Controls on Runoff and Low  
1060 Flows in Mountain Catchments of Western North America. *Water Resources Research*,  
1061 54(10), 7495–7510. <https://doi.org/10.1029/2018WR023087>
- 1062 Faunt, C.C., Belitz, K., Hanson, R.T., 2010. Development of a three-dimensional model of  
1063 sedimentary texture in valley-fill deposits of Central Valley, California, USA.  
1064 *Hydrogeology Journal* 18, 625–649. <https://doi.org/10.1007/s10040-009-0539-7>



- 1065 Faunt, C.C., Geological Survey (U.S.) (Eds.), 2009. Groundwater availability of the Central Valley  
1066 Aquifer, California, U.S. Geological Survey professional paper. U.S. Geological Survey,  
1067 Reston, Va.
- 1068 Ficklin, D. L., Luo, Y., & Zhang, M. (2013). Climate change sensitivity assessment of streamflow  
1069 and agricultural pollutant transport in California's Central Valley using Latin hypercube  
1070 sampling. *Hydrological Processes*, 27(18), 2666–2675. <https://doi.org/10.1002/hyp.9386>
- 1071 Foster, L. M., Williams, K. H., & Maxwell, R. M. (2020). Resolution matters when modeling  
1072 climate change in headwaters of the Colorado River. *Environmental Research Letters*.  
1073 <https://doi.org/10.1088/1748-9326/aba77f>
- 1074 Gates WL (1992) AMIP: the atmospheric model intercomparison project. *Bull Am Meteorol Soc*  
1075 73(12):1962–1970. doi:10.1175/1520-0477(1992)073<1962:ATAMIP>2.0.CO;2
- 1076 Geologic Map of California, 2015. Geologic Map of California [WWW Document]. Geologic Map  
1077 of California. URL <https://maps.conservation.ca.gov/cgs/gmc/> (accessed 10.17.18).
- 1078 Gent, P. R., Danabasoglu, G., Donner, L. J., Holland, M. M., Hunke, E. C., Jayne, S. R., et al.  
1079 (2011). The Community Climate System Model Version 4. *Journal of Climate*, 24(19),  
1080 4973–4991. <https://doi.org/10.1175/2011JCLI4083.1>
- 1081 Gershunov, A., Shulgina, T., Clemesha, R.E.S. et al. (2019). Precipitation regime change in  
1082 Western North America: The role of Atmospheric Rivers. *Sci Rep* 9, 9944.  
1083 <https://doi.org/10.1038/s41598-019-46169-w>
- 1084 Gettelman, A., and Morrison, H. (2015). Advanced Two-Moment Bulk Microphysics for Global  
1085 Models. Part I: Off-Line Tests and Comparison with Other Schemes. *Journal of Climate*  
1086 28, 3, 1268-1287. <https://doi.org/10.1175/JCLI-D-14-00102.1>



- 1087 Gilbert, J.M., Maxwell, R.M., 2017. Examining regional groundwater - surface water dynamics  
1088 using an integrated hydrologic model of the San Joaquin River basin. *Hydrology and Earth*  
1089 *System Sciences* 21, 923–947. <https://doi.org/10.5194/hess-21-923-2017>
- 1090 Gleick, P. H. (1987). The development and testing of a water balance model for climate impact  
1091 assessment: Modeling the Sacramento Basin. *Water Resources Research*, 23(6), 1049–  
1092 1061. <https://doi.org/10.1029/WR023i006p01049>
- 1093 Godsey, S. E., Kirchner, J. W., & Tague, C. L. (2014). Effects of changes in winter snowpacks on  
1094 summer low flows: case studies in the Sierra Nevada, California, USA. *Hydrological*  
1095 *Processes*, 28(19), 5048–5064. <https://doi.org/10.1002/hyp.9943>
- 1096 Griffin, D., & Anchukaitis, K. J. (2014). How unusual is the 2012–2014 California drought?  
1097 *Geophysical Research Letters*, 41(24), 9017–9023.  
1098 <https://doi.org/10.1002/2014GL062433>
- 1099 Haarsma, R. J., Roberts, M. J., Vidale, P. L., Senior, C. A., Bellucci, A., Bao, Q., Chang, P., Corti,  
1100 S., Fučkar, N. S., Guemas, V., von Hardenberg, J., Hazeleger, W., Kodama, C., Koenigk,  
1101 T., Leung, L. R., Lu, J., Luo, J.-J., Mao, J., Mizielinski, M. S., Mizuta, R., Nobre, P., Satoh,  
1102 M., Scoccimarro, E., Semmler, T., Small, J., and von Storch, J.-S. (2016). High Resolution  
1103 Model Intercomparison Project (HighResMIP v1.0) for CMIP6, *Geosci. Model Dev.*, 9,  
1104 4185–4208, <https://doi.org/10.5194/gmd-9-4185-2016>.
- 1105 Harpold, A. A., & Molotch, N. P. (2015). Sensitivity of soil water availability to changing  
1106 snowmelt timing in the western U.S. *Geophysical Research Letters*, 42(19), 8011–8020.  
1107 <https://doi.org/10.1002/2015GL065855>
- 1108 Hayhoe, K., Cayan, D., Field, C. B., Frumhoff, P. C., Maurer, E. P., Miller, N. L., et al. (2004).  
1109 Emissions pathways, climate change, and impacts on California. *Proceedings of the*



- 1110 *National Academy of Sciences*, 101(34), 12422–12427.  
1111 <https://doi.org/10.1073/pnas.0404500101>
- 1112 He, M., Anderson, M., Schwarz, A., Das, T., Lynn, E., Anderson, J., et al. (2019). Potential  
1113 Changes in Runoff of California’s Major Water Supply Watersheds in the 21st Century.  
1114 *Water*, 11(8), 1651. <https://doi.org/10.3390/w11081651>
- 1115 Herrington, A. R., P. H. Lauritzen, M. A. Taylor, S. Goldhaber, B. E. Eaton, J. T. Bacmeister, K.  
1116 A. Reed, and P. A. Ullrich (2019). Physics–Dynamics Coupling with Element-Based High-  
1117 Order Galerkin Methods: Quasi-Equal-Area Physics Grid. *Mon. Wea. Rev.*, 147, 69–84,  
1118 <https://doi.org/10.1175/MWR-D-18-0136.1>.
- 1119 Homer, C., Dewitz, J., Yang, L., Jin, S., Danielson, P., Xian, G., et al. (2015). Completion of the  
1120 2011 National Land Cover Database for the conterminous United States—representing a  
1121 decade of land cover change information. *Photogrammetric Engineering & Remote*  
1122 *Sensing*, 81(5), 345–354.
- 1123 Huang, X., Rhoades, A. M., Ullrich, P. A., & Zarzycki, C. M. (2016). An evaluation of the  
1124 variable-resolution CESM for modeling California’s climate. *Journal of Advances in*  
1125 *Modeling Earth Systems*, 8(1), 345–369. <https://doi.org/10.1002/2015MS000559>
- 1126 Huang, X., Stevenson, S., & Hall, A. D. (2020). Future warming and intensification of  
1127 precipitation extremes: A “double whammy” leading to increasing flood risk in California.  
1128 *Geophysical Research Letters*, 47, e2020GL088679.  
1129 <https://doi.org/10.1029/2020GL088679>
- 1130 Hurrell, J. W., Holland, M. M., Gent, P. R., Ghan, S., Kay, J. E., Kushner, P. J., et al. (2013). The  
1131 Community Earth System Model: A Framework for Collaborative Research. *Bulletin of*





- 1132            *the American Meteorological Society*, 94(9), 1339–1360. <https://doi.org/10.1175/BAMS->  
1133            D-12-00121.1
- 1134 Jones, P. W., (1999). First- and Second-Order Conservative Remapping Schemes for Grids in  
1135            Spherical Coordinates. *Mon. Wea. Rev.*, 127, 2204–2210, <https://doi.org/10.1175/1520->  
1136            [0493\(1999\)127<2204:FASOCR>2.0.CO;2](https://doi.org/10.1175/1520-0493(1999)127<2204:FASOCR>2.0.CO;2).
- 1137 IGBP, 2018. Global plant database published - IGBP [WWW Document]. URL  
1138            <http://www.igbp.net/news/news/news/globalplantdatabasepublished.5.1b8ae20512db692f>  
1139            [2a6800014762.html](http://www.igbp.net/news/news/news/globalplantdatabasepublished.5.1b8ae20512db692f) (accessed 10.17.18).
- 1140 Jennings, C. W., Strand, R. G., & Rogers, T. H. (1977). Geologic map of California. Sacramento,  
1141            Calif.: Division of Mines and Geology.
- 1142 Kampenhout, L. van, Rhoades, A. M., Herrington, A. R., Zarzycki, C. M., Lenaerts, J. T. M.,  
1143            Sacks, W. J., & Broeke, M. R. van den. (2019). Regional grid refinement in an Earth system  
1144            model: impacts on the simulated Greenland surface mass balance. *The Cryosphere*, 13(6),  
1145            1547–1564. <https://doi.org/10.5194/tc-13-1547-2019>
- 1146 Kollet, S. J., & Maxwell, R. M. (2006). Integrated surface–groundwater flow modeling: A free-  
1147            surface overland flow boundary condition in a parallel groundwater flow model. *Advances*  
1148            *in Water Resources*, 29(7), 945–958. <https://doi.org/10.1016/j.advwatres.2005.08.006>
- 1149 Lemordant, L., Gentine, P., Swann, A. S., Cook, B. I., & Scheff, J. (2018). Critical impact of  
1150            vegetation physiology on the continental hydrologic cycle in response to increasing CO<sub>2</sub>.  
1151            *Proceedings of the National Academy of Sciences*, 115(16), 4093–4098.  
1152            <https://doi.org/10.1073/pnas.1720712115>
- 1153 Lundquist, J. D., Hughes, M., Henn, B., Gutmann, E. D., Livneh, B., Dozier, J., & Neiman, P.  
1154            (2015). High-Elevation Precipitation Patterns: Using Snow Measurements to Assess Daily



- 1155 Gridded Datasets across the Sierra Nevada, California, *Journal of Hydrometeorology*,  
1156 16(4), 1773-1792. doi: [https://journals.ametsoc.org/view/journals/hydr/16/4/jhm-d-15-](https://journals.ametsoc.org/view/journals/hydr/16/4/jhm-d-15-0019_1.xml)  
1157 0019\_1.xml
- 1158 Maina, Fadji Z., Siirila-Woodburn, E. R., Newcomer, M., Xu, Z., & Steefel, C. (2020a).  
1159 Determining the impact of a severe dry to wet transition on watershed hydrodynamics in  
1160 California, USA with an integrated hydrologic model. *Journal of Hydrology*, 580, 124358.  
1161 <https://doi.org/10.1016/j.jhydrol.2019.124358>
- 1162 Maina, F. Z., Siirila-Woodburn, E. R., & Vahmani, P. (2020b). Sensitivity of meteorological-  
1163 forcing resolution on hydrologic variables. *Hydrology and Earth System Sciences*, 24(7),  
1164 3451–3474. <https://doi.org/10.5194/hess-24-3451-2020>
- 1165 Maina, Fadji Zaouna, & Siirila-Woodburn, E. R. (2020c). Watersheds dynamics following  
1166 wildfires: Nonlinear feedbacks and implications on hydrologic responses. *Hydrological*  
1167 *Processes*, 34(1), 33–50. <https://doi.org/10.1002/hyp.13568>
- 1168 Mallakpour, I., Sadegh, M., AghaKouchak, A., 2018. A new normal for streamflow in California  
1169 in a warming climate: Wetter wet seasons and drier dry seasons. *Journal of Hydrology* 567,  
1170 203–211. <https://doi.org/10.1016/j.jhydrol.2018.10.023>
- 1171 Maurer, E. P. (2007). Uncertainty in hydrologic impacts of climate change in the Sierra Nevada,  
1172 California, under two emissions scenarios. *Climatic Change*, 82(3), 309–325.  
1173 <https://doi.org/10.1007/s10584-006-9180-9>
- 1174 Maurer, E. P., & Duffy, P. B. (2005). Uncertainty in projections of streamflow changes due to  
1175 climate change in California. *Geophysical Research Letters*, 32(3).  
1176 <https://doi.org/10.1029/2004GL021462>



- 1177 Maxwell, R. M. (2013). A terrain-following grid transform and preconditioner for parallel, large-  
1178 scale, integrated hydrologic modeling. *Advances in Water Resources*, 53, 109–117.  
1179 <https://doi.org/10.1016/j.advwatres.2012.10.001>
- 1180 Maxwell, R. M., & Condon, L. E. (2016). Connections between groundwater flow and  
1181 transpiration partitioning. *Science*, 353(6297), 377–380.  
1182 <https://doi.org/10.1126/science.aaf7891>
- 1183 Maxwell, R. M., & Miller, N. L. (2005). Development of a Coupled Land Surface and  
1184 Groundwater Model. *Journal of Hydrometeorology*, 6(3), 233–247.  
1185 <https://doi.org/10.1175/JHM422.1>
- 1186 Mayer, T. D., & Naman, S. W. (2011). Streamflow Response to Climate as Influenced by Geology  
1187 and Elevation1. *JAWRA Journal of the American Water Resources Association*, 47(4),  
1188 724–738. <https://doi.org/10.1111/j.1752-1688.2011.00537.x>Boryan, C., Yang, Z.,  
1189 Mueller, R., Craig, M., 2011. Monitoring US agriculture: the US Department of  
1190 Agriculture, National Agricultural Statistics Service, Cropland Data Layer Program.  
1191 Geocarto International 26, 341–358. <https://doi.org/10.1080/10106049.2011.562309>
- 1192 Mallakpour, I., Sadegh, M., AghaKouchak, A., 2018. A new normal for streamflow in California  
1193 in a warming climate: Wetter wet seasons and drier dry seasons. *Journal of Hydrology* 567,  
1194 203–211. <https://doi.org/10.1016/j.jhydrol.2018.10.023>
- 1195 Maxwell, R.M., 2013. A terrain-following grid transform and preconditioner for parallel, large-  
1196 scale, integrated hydrologic modeling. *Advances in Water Resources* 53, 109–117.  
1197 <https://doi.org/10.1016/j.advwatres.2012.10.001>
- 1198 McEvoy, D.J., Pierce, D.W., Kalansky, J.F., Cayan, D.R., Abatzoglou, J.T., 2020. Projected  
1199 Changes in Reference Evapotranspiration in California and Nevada: Implications for



- 1200 Drought and Wildland Fire Danger. *Earth's Future* 8, e2020EF001736.  
1201 <https://doi.org/10.1029/2020EF001736>
- 1202 Welch, L.A., Allen, D.M., 2014. Hydraulic conductivity characteristics in mountains and  
1203 implications for conceptualizing bedrock groundwater flow. *Hydrogeol J* 22, 1003–1026.  
1204 <https://doi.org/10.1007/s10040-014-1121-5>
- 1205 Milly, P. C. D., & Dunne, K. A. (2017). A Hydrologic Drying Bias in Water-Resource Impact  
1206 Analyses of Anthropogenic Climate Change. *JAWRA Journal of the American Water*  
1207 *Resources Association*, 53(4), 822–838. <https://doi.org/10.1111/1752-1688.12538>
- 1208 Milly, P. C. D., Dunne, K. A., & Vecchia, A. V. (2005). Global pattern of trends in streamflow  
1209 and water availability in a changing climate. *Nature*, 438(7066), 347–350.  
1210 <https://doi.org/10.1038/nature04312>
- 1211 Mote, P. W., Hamlet, A. F., Clark, M. P., & Lettenmaier, D. P. (2005). Declining mountain  
1212 snowpack in western north america\*. *Bulletin of the American Meteorological Society*,  
1213 86(1), 39–50. <https://doi.org/10.1175/BAMS-86-1-39>
- 1214 Musselman, K. N., Clark, M. P., Liu, C., Ikeda, K., & Rasmussen, R. (2017). Slower snowmelt in  
1215 a warmer world. *Nature Climate Change*, 7(3), 214–219.  
1216 <https://doi.org/10.1038/nclimate3225>
- 1217 Musselman, K. N., Molotch, N. P., & Margulis, S. A. (2017). Snowmelt response to simulated  
1218 warming across a large elevation gradient, southern Sierra Nevada, California. *The*  
1219 *Cryosphere*, 11(6), 2847–2866. <https://doi.org/10.5194/tc-11-2847-2017>
- 1220 Neelin, J. D., Langenbrunner, B., Meyerson, J. E., Hall, A., & Berg, N. (2013). California Winter  
1221 Precipitation Change under Global Warming in the Coupled Model Intercomparison



- 1222 Project Phase 5 Ensemble. *Journal of Climate*, 26(17), 6238–6256.  
1223 <https://doi.org/10.1175/JCLI-D-12-00514.1>
- 1224 Niraula, R., Meixner, T., Dominguez, F., Bhattarai, N., Rodell, M., Ajami, H., et al. (2017). How  
1225 Might Recharge Change Under Projected Climate Change in the Western U.S.?  
1226 *Geophysical Research Letters*, 44(20), 10,407–10,418.  
1227 <https://doi.org/10.1002/2017GL075421>
- 1228 Pascolini-Campbell, M., Reager, J. T., Chandanpurkar, H. A., & Rodell, M. (2021). A 10 per cent  
1229 increase in global land evapotranspiration from 2003 to 2019. *Nature*, 593(7860), 543–547.  
1230 <https://doi.org/10.1038/s41586-021-03503-5>
- 1231 Payne, A. E., Demory, M.-E., Leung, L. R., Ramos, A. M., Shields, C. A., Rutz, J. J., et al. (2020).  
1232 Responses and impacts of atmospheric rivers to climate change. *Nature Reviews Earth &*  
1233 *Environment*, 1(3), 143–157. <https://doi.org/10.1038/s43017-020-0030-5>
- 1234 Persad, G. G., Swain, D. L., Kouba, C., & Ortiz-Partida, J. P. (2020). Inter-model agreement on  
1235 projected shifts in California hydroclimate characteristics critical to water management.  
1236 *Climatic Change*, 162(3), 1493–1513. <https://doi.org/10.1007/s10584-020-02882-4>
- 1237 Ralph, F. M., & Dettinger, M. D. (2011). Storms, floods, and the science of atmospheric rivers.  
1238 *Eos, Transactions American Geophysical Union*, 92(32), 265–266.  
1239 <https://doi.org/10.1029/2011EO320001>
- 1240 Ralph, F. Martin, Neiman, P. J., Wick, G. A., Gutman, S. I., Dettinger, M. D., Cayan, D. R., &  
1241 White, A. B. (2006). Flooding on California’s Russian River: Role of atmospheric rivers.  
1242 *Geophysical Research Letters*, 33(13). <https://doi.org/10.1029/2006GL026689>
- 1243 Rasmussen, R., Liu, C., Ikeda, K., Gochis, D., Yates, D., Chen, F., et al. (2011). High-Resolution  
1244 Coupled Climate Runoff Simulations of Seasonal Snowfall over Colorado: A Process



- 1245 Study of Current and Warmer Climate. *Journal of Climate*, 24(12), 3015–3048.  
1246 <https://doi.org/10.1175/2010JCLI3985.1>
- 1247 Rhoades, A. M., Huang, X., Ullrich, P. A., & Zarzycki, C. M. (2016). Characterizing Sierra Nevada  
1248 Snowpack Using Variable-Resolution CESM. *Journal of Applied Meteorology and*  
1249 *Climatology*, 55(1), 173–196. <https://doi.org/10.1175/JAMC-D-15-0156.1>
- 1250 Rhoades, A. M., Ullrich, P. A., & Zarzycki, C. M. (2018a). Projecting 21st century snowpack  
1251 trends in western USA mountains using variable-resolution CESM. *Climate Dynamics*,  
1252 50(1), 261–288. <https://doi.org/10.1007/s00382-017-3606-0>
- 1253 Rhoades, A. M., Jones, A. D., & Ullrich, P. A. (2018b). The changing character of the California  
1254 Sierra Nevada as a natural reservoir. *Geophysical Research Letters*, 45, 13,008– 13,019.  
1255 <https://doi.org/10.1029/2018GL080308>
- 1256 Rhoades, A. M., Ullrich, P. A., Zarzycki, C. M., Johansen, H., Margulis, S. A., Morrison, H., et  
1257 al. (2018c). Sensitivity of Mountain Hydroclimate Simulations in Variable-Resolution  
1258 CESM to Microphysics and Horizontal Resolution. *Journal of Advances in Modeling Earth*  
1259 *Systems*, 10(6), 1357–1380. <https://doi.org/10.1029/2018MS001326>
- 1260 Rhoades, A. M., Jones, A. D., O'Brien, T. A., O'Brien, J. P., Ullrich, P. A., & Zarzycki, C. M.  
1261 (2020a). Influences of North Pacific Ocean domain extent on the western U.S. winter  
1262 hydroclimatology in variable-resolution CESM. *Journal of Geophysical Research:*  
1263 *Atmospheres*, 125, e2019JD031977. <https://doi.org/10.1029/2019JD031977>
- 1264 Rhoades, A. M., Jones, A. D., Srivastava, A., Huang, H., O'Brien, T. A., Patricola, C. M., et al.  
1265 (2020b). The shifting scales of western U.S. landfalling atmospheric rivers under climate  
1266 change. *Geophysical Research Letters*, 47, e2020GL089096.  
1267 <https://doi.org/10.1029/2020GL089096>



- 1268 Rhoades, A. M., Risser, M. D., Stone, D. A., Wehner, M. F., & Jones, A. D. (2021). Implications  
1269 of warming on western United States landfalling atmospheric rivers and their flood  
1270 damages. *Weather and Climate Extremes*, 32, 100326,  
1271 <https://doi.org/10.1016/j.wace.2021.100326>
- 1272 Richards, L. A. (1931). Capillary conduction of liquids through porous medium. *Journal of*  
1273 *Applied Physics*, 1(5), 318–333. <https://doi.org/10.1063/1.1745010>
- 1274 Safeeq, M., Grant, G. E., Lewis, S. L., Kramer, M. G., & Staab, B. (2014). A hydrogeologic  
1275 framework for characterizing summer streamflow sensitivity to climate warming in the  
1276 Pacific Northwest, USA. *Hydrology and Earth System Sciences*, (18), 1–8.  
1277 <https://doi.org/10.5194/hess-18-3693-2014>
- 1278 Safeeq, M., Grant, G.E., Lewis, S.L. and Tague, C.L. (2013), Coupling snowpack and groundwater  
1279 dynamics to interpret historical streamflow trends in the western United States. *Hydrol.*  
1280 *Process.*, 27: 655-668. <https://doi.org/10.1002/hyp.9628>
- 1281 Safeeq, Mohammad, Grant, G. E., Lewis, S. L., & Staab, B. (2015). Predicting landscape  
1282 sensitivity to present and future floods in the Pacific Northwest, USA. *Hydrological*  
1283 *Processes*, 29(26), 5337–5353. <https://doi.org/10.1002/hyp.10553>
- 1284 SCRIPPS Institution of Oceanography. (2017, April). Northern California Just Surpassed the  
1285 Wettest Year on Record | Scripps Institution of Oceanography, UC San Diego. Retrieved  
1286 from <https://scripps.ucsd.edu/news/northern-california-just-surpassed-wettest-year-record>
- 1287 Shukla, S., Safeeq, M., AghaKouchak, A., Guan, K., & Funk, C. (2015). Temperature impacts on  
1288 the WY 2014 drought in California. *Geophysical Research Letters*, 4384–4393.  
1289 [https://doi.org/10.1002/2015GL063666@10.1002/\(ISSN\)1944-8007.CALDROUGHT1](https://doi.org/10.1002/2015GL063666@10.1002/(ISSN)1944-8007.CALDROUGHT1)



- 1290 Son, K., & Tague, C. (2019). Hydrologic responses to climate warming for a snow-dominated  
1291 watershed and a transient snow watershed in the California Sierra. *Ecohydrology*, *12*(1),  
1292 e2053. <https://doi.org/10.1002/eco.2053>
- 1293 Strachan, S., and Daly, C. (2017), Testing the daily PRISM air temperature model on semiarid  
1294 mountain slopes, *J. Geophys. Res. Atmos.*, *122*, 5697– 5715, doi:10.1002/2016JD025920.
- 1295 Swain, D. L., Langenbrunner, B., Neelin, J. D., & Hall, A. (2018). Increasing precipitation  
1296 volatility in twenty-first-century California. *Nature Climate Change*, *8*(5), 427–433.  
1297 <https://doi.org/10.1038/s41558-018-0140-y>
- 1298 Tague, C., & Peng, H. (2013). The sensitivity of forest water use to the timing of precipitation and  
1299 snowmelt recharge in the California Sierra: Implications for a warming climate. *Journal of*  
1300 *Geophysical Research: Biogeosciences*, *118*(2), 875–887.  
1301 <https://doi.org/10.1002/jgrg.20073>
- 1302 Tang, G., Li, S., Yang, M., Xu, Z., Liu, Y., & Gu, H. (2019). Streamflow response to snow regime  
1303 shift associated with climate variability in four mountain watersheds in the US Great Basin.  
1304 *Journal of Hydrology*, *573*, 255–266. <https://doi.org/10.1016/j.jhydrol.2019.03.021>
- 1305 The NCAR Command Language (Version 6.6.2) (2021). Boulder, Colorado:  
1306 UCAR/NCAR/CISL/TDD, 851 <http://dx.doi.org/10.5065/D6WD3XH5>.
- 1307 Vicuna, S., & Dracup, J. A. (2007). The evolution of climate change impact studies on hydrology  
1308 and water resources in California. *Climatic Change*, *82*(3), 327–350.  
1309 <https://doi.org/10.1007/s10584-006-9207-2>
- 1310 Vicuna, Sebastian, Maurer, E. P., Joyce, B., Dracup, J. A., & Purkey, D. (2007). The Sensitivity  
1311 of California Water Resources to Climate Change Scenarios<sup>1</sup>. *JAWRA Journal of the*





1312            *American Water Resources Association*, 43(2), 482–498. <https://doi.org/10.1111/j.1752->  
1313            1688.2007.00038.x

1314    Wang, S.-Y. S., Yoon, J.-H., Becker, E., & Gillies, R. (2017). California from drought to deluge.  
1315            *Nature Climate Change*, 7(7), 465. <https://doi.org/10.1038/nclimate3330>

1316    Wu, C., Liu, X., Lin, Z., Rhoades, A. M., Ullrich, P. A., Zarzycki, C. M., et al. (2017). Exploring  
1317            a Variable-Resolution Approach for Simulating Regional Climate in the Rocky Mountain  
1318            Region Using the VR-CESM. *Journal of Geophysical Research: Atmospheres*, 122(20),  
1319            10,939–10,965. <https://doi.org/10.1002/2017JD027008>

1320    Zarzycki, C. M., Levy, M. N., Jablonowski, C., Overfelt, J. R., Taylor, M. A., and Ullrich, P. A.  
1321            (2014). Aquaplanet Experiments Using CAM’s Variable-Resolution Dynamical Core.  
1322            *Journal of Climate* 27, 14, 5481–5503, <https://doi.org/10.1175/JCLI-D-14-00004.1>

1323

1324

1325

1326